







# BCL11B and the NuRD complex cooperatively guard T-cell fate and inhibit OPA1-mediated mitochondrial fusion in T cells

Rui Liao<sup>1,†</sup> , Yi Wu<sup>1,†</sup> , Le Qin<sup>1</sup>, Zhiwu Jiang<sup>1</sup>, Shixue Gou<sup>1</sup>, Linfu Zhou<sup>1</sup>, Qilan Hong<sup>2,3</sup>, Yao Li<sup>1</sup>, Jingxuan Shi<sup>1</sup>, Yao Yao<sup>1</sup>, Liangxue Lai<sup>1</sup>, Yangqiu Li<sup>4</sup> , Pentao Liu<sup>5</sup>, Jean Paul Thiery<sup>6</sup>, Dajiang Qin<sup>7</sup>, Thomas Graf<sup>2,3</sup> , Xingguo Liu<sup>1,8,\*</sup>  & Peng Li<sup>1,7,8,9,\*\*</sup> 

## Abstract

The nucleosome remodeling and histone deacetylase (NuRD) complex physically associates with BCL11B to regulate murine T-cell development. However, the function of NuRD complex in mature T cells remains unclear. Here, we characterize the fate and metabolism of human T cells in which key subunits of the NuRD complex or BCL11B are ablated. BCL11B and the NuRD complex bind to each other and repress natural killer (NK)-cell fate in T cells. In addition, T cells upregulate the NK cell-associated receptors and transcription factors, lyse NK-cell targets, and are reprogrammed into NK-like cells (ITNKs) upon deletion of MTA2, MBD2, CHD4, or BCL11B. ITNKs increase OPA1 expression and exhibit characteristically elongated mitochondria with augmented oxidative phosphorylation (OXPHOS) activity. OPA1-mediated elevated OXPHOS enhances cellular acetyl-CoA levels, thereby promoting the reprogramming efficiency and antitumor effects of ITNKs via regulating H3K27 acetylation at specific targets. In conclusion, our findings demonstrate that the NuRD complex and BCL11B cooperatively maintain T-cell fate directly by repressing NK cell-associated transcription and indirectly through a metabolic-epigenetic axis, providing strategies to improve the reprogramming efficiency and antitumor effects of ITNKs.

**Keywords** CHD4; MBD2; MTA2; OPA1; T-cell fate

**Subject Categories** Cancer; Immunology; Metabolism

DOI 10.15252/emj.2023113448 | Received 5 January 2023 | Revised 13 August 2023 | Accepted 17 August 2023 | Published online 22 September 2023

The EMBO Journal (2023) 42: e113448

## Introduction

Bcl11b is a transcription factor for murine T-cell commitment (Ikawa *et al.*, 2010; Li *et al.*, 2010a, 2010b; Isoda *et al.*, 2017; Hosokawa *et al.*, 2018; Hu *et al.*, 2018) and directly represses the transcription of Id2 and Zbtb16, which are essential for NK cell development (Constantinides *et al.*, 2014; Delconte *et al.*, 2016; Hosokawa *et al.*, 2018, 2020). Other groups and we reported that inactivating BCL11B in human T cells induces their reprogramming into NK-like cells (induced T-to-NK cells, ITNKs) (Maluski *et al.*, 2019; Sottile *et al.*, 2021; Wu *et al.*, 2021; Jiang *et al.*, 2022). ITNKs retain the expression of a diverse TCR repertoire and upregulate NK-cell-associated markers and transcription factors. In addition, ITNKs recognize and lyse tumor cells efficiently *in vitro* and *in vivo*. Preliminary clinical results (NCT:03882840) show that autologous ITNKs provide modest benefits in patients with refractory and advanced solid tumors without causing severe adverse effects (Jiang *et al.*, 2022).

BCL11B physically associates with the nucleosome remodeling and histone deacetylase (NuRD) complex, a major transcriptional corepressor, via interaction with MTA1 and MTA2 to repress the expression of downstream targets, including HIV-1 LTR, Id2, and

- China-New Zealand Joint Laboratory of Biomedicine and Health, State Key Laboratory of Respiratory Disease, Guangdong Provincial Key Laboratory of Stem Cell and Regenerative Medicine, CAS Key Laboratory of Regenerative Biology, GIBH-HKU Guangdong-Hong Kong Stem Cell and Regenerative Medicine Research Centre, GIBH-CUHK Joint Research Laboratory on Stem Cell and Regenerative Medicine, Guangzhou Institutes of Biomedicine and Health, Chinese Academy of Sciences, Guangzhou, China
  - Bioland Laboratory (Guangzhou Regenerative Medicine and Health Guangdong Laboratory), Guangzhou, China
  - Centre for Genomic Regulation, The Barcelona Institute of Science and Technology, Barcelona, Spain
  - Institute of Hematology, Medical College, Jinan University, Guangzhou, China
  - School of Biomedical Sciences, Stem Cell and Regenerative Medicine Consortium, Li Ka Shing Faculty of Medicine, The University of Hong Kong, Hong Kong SAR, China
  - Guangzhou Laboratory, Guangzhou, China
  - Key Laboratory of Biological Targeting Diagnosis, Therapy, and Rehabilitation of Guangdong Higher Education Institutes, The Fifth Affiliated Hospital of Guangzhou Medical University, Guangzhou, China
  - Centre for Regenerative Medicine and Health, Hong Kong Institute of Science & Innovation, Chinese Academy of Sciences, Hong Kong SAR, China
  - Department of Surgery, The Chinese University of Hong Kong, Hong Kong SAR, China
- \*Corresponding author. Tel: +86 18688900777; E-mail: liu\_xingguo@gibh.ac.cn  
 \*\*Corresponding author. Tel: +86 18026219834; E-mail: li\_peng@gibh.ac.cn  
 †These authors contributed equally to this work

Cdkn1c in T cells (Cismasiu *et al.*, 2005, 2008; Topark-Ngarm *et al.*, 2006; Dubuissez *et al.*, 2016; Hosokawa *et al.*, 2018). The NuRD complex also plays essential roles in T-cell fate and immune response (Lu *et al.*, 2008; Rothenberg, 2012; Dege & Hagman, 2014; Loughran *et al.*, 2017; Shen *et al.*, 2018). It is a critical cofactor binding to transcription factors to control T-cell differentiation (Gao *et al.*, 2022b). Ablation of *Mta2* derepresses the expression of genes that are directly bound to and repressed by *Bcl11b* in murine T cells (Hosokawa *et al.*, 2018). However, it remains to assess the function of the NuRD complex and *BCL11B* in maintaining T cell identity.

Mitochondria are highly dynamic organelles that undergo fission and fusion and provide energy for cellular activities, including T cell development and function (Ghesquière *et al.*, 2014; Dimeloe *et al.*, 2017). T cells exhibit unique metabolic profiles in different states (MacIver *et al.*, 2013; Kishton *et al.*, 2017). Naïve T (Tn) cells remain in a quiescent state through oxidative phosphorylation (OXPHOS) and fatty acid oxidation (FAO), while effector T (Te) cells upregulate aerobic glycolysis to support differentiation and rapid proliferation with activation (Chang *et al.*, 2013). When antigens are cleared, long-lived memory T (Tm) cells facilitate OXPHOS and FAO to meet energy requirements (van der Windt *et al.*, 2012; Sukumar *et al.*, 2013; O'Sullivan *et al.*, 2014). Memory T cells rely on FAO to fuel OXPHOS, in which mitochondria fuse to form linear or tubular networks. At the same time, mitochondria can also undergo fission, generating discrete and fragmented mitochondria in activated T cells (West *et al.*, 2011; Buck *et al.*, 2016; Kishton *et al.*, 2017). Mitochondrial fusion is mediated by outer membrane fusion proteins (mitofusin1 and mitofusin2) and inner membrane fusion proteins (optic atrophy 1, OPA1) (Chen *et al.*, 2003; Song *et al.*, 2009; Kishton *et al.*, 2017). OPA1-mediated mitochondrial fusion enhances FAO and OXPHOS metabolism in Tm cells (Buck *et al.*, 2016; Kishton *et al.*, 2017). Alternative splicing of OPA1 gives rise to long forms that can be cleaved into short forms by peptidases (Ishihara *et al.*, 2006; Del Dotto *et al.*, 2018). The presence of long-(L) and short-form (S)-OPA1 is necessary for mitochondrial dynamics (Song *et al.*, 2007). L-OPA1 is indispensable for mitochondrial fusion, while S-OPA1 promotes mitochondrial fragmentation (Anand *et al.*, 2014; Baker *et al.*, 2014). In contrast, dynamin-related protein 1 (Drp1), a mitochondrial fission protein, regulates mitochondrial fragmentation to decrease OXPHOS metabolism through phosphorylation (Losón *et al.*, 2013; Sukumar *et al.*, 2013).

To understand the NuRD complex function in mature T cells, we ablated *MTA2*, *MBD2*, and *CHD4*, three critical subunits of the NuRD complex, individually in human primary T cells using CRISPR/Cas9 and characterized the transcription profiles and cytotoxicity of these genetically modified T cells. We also studied how *BCL11B* and the NuRD complex control the morphology and function of mitochondria in T cells.

## Results

### Ablation of subunits of the NuRD complex reprograms human T cells into ITNKs

To investigate whether *BCL11B* associates with the NuRD complex to maintain T-cell identity, we performed coimmunoprecipitation

(co-IP) assays in human T cells and found that NuRD subunits, including *MTA2*, *MBD2*, and *CHD4*, physically interact with *BCL11B* (Fig 1A). We next ablated *MTA2*, *MBD2*, or *CHD4* individually with the CRISPR/Cas9 technology in primary human T cells and cultured them with standard T-cell culture conditions (Appendix Fig S1A). Like *sgBCL11B*-transduced T cells, cultured *sgMTA2*-transduced T cells showed  $CD8^+NKp46^+$  and  $CD4^+NKp30^+$  populations, although the percentages of  $CD8^+NKp46^+$  and  $CD4^+NKp30^+$  cells were lower in *sgMTA2*-transduced T cells than in *sgBCL11B*-transduced T cells (Fig 1B and C). In cultures of *sgMBD2*-transduced or *sgCHD4*-transduced T cells, *NKp30* expression was significantly upregulated in both  $CD4^+$  and  $CD8^+$  T cells as compared to *sgCtrl* T cells, although fewer  $CD8^+NKp46^+$  cells were detected (Fig 1B and C). In contrast, the ablation of *MTA1*, another component of the NuRD complex, did not alter the expression of *NKp30* or *NKp46* in T cells (Appendix Fig S1B). In addition, *sgBCL11B*-, *sgMTA2*-, *sgMBD2*-, and *sgCHD4*-transduced T cells efficiently lysed K562 cells *in vitro* (Fig 1D), suggesting that these cells recognized NK-cell targets. Collectively, these results show that human primary T cells can be reprogrammed into ITNKs when lacking subunits of the NuRD complex.

### *BCL11B* associates with the NuRD complex to repress the expression of NK-cell-associated genes in human T cells

To further understand the characteristics of NuRD complex-deficient ITNKs,  $CD8^+NKp30^+$  and  $CD4^+NKp30^+$  populations from *BCL11B*-, *MTA2*-, *MBD2*-, and *CHD4*-deficient ITNKs were purified and subjected to RNA-sequencing (RNA-seq) analysis. The transcriptional profiles of ITNKs derived from *sgMTA2*-, *sgMBD2*-, and *sgCHD4*-transduced T cells were like those of *sgBCL11B*-transduced T cells but not to those of *sgCtrl*-transduced T cells (Figs 2A and EV1A and B). Gene Ontology (G.O.) enrichment analysis showed that derepressed genes in both  $CD4^+$  and  $CD8^+$  populations in *sgMTA2*-, *sgMBD2*-, *sgCHD4*-, and *sgBCL11B*-transduced T cells as compared to *sgCtrl*-transduced T cells were enriched in genes related to T-cell activation and NK-cell-mediated immunity (Fig EV1C and D). In addition, there were 450 and 172 Differentially Expressed Genes (DEGs), including *ID2*, *ZNF683*, and *ITGAX* encoding *CD11C*, *FCER1G*, and *TNFRSF18*, that were derepressed in *sgBCL11B*-, *sgMTA2*-, *sgMBD2*-, and *sgCHD4*-transduced  $CD8^+$  and  $CD4^+$  T cells, respectively, compared to control T cells (Fig 2B and C). These analyses demonstrate that ITNKs generated from *MTA2*-, *MBD2*-, and *CHD4*-deficient T cells share similar gene expression profiles with *BCL11B*-deficient ITNKs in T-cell activation and NK-cell-mediated immunity.

$CD4^+$  cytotoxic T lymphocytes ( $CD4$ -CTLs), which are essential for immune responses to various viral infections (Juno *et al.*, 2017; Takeuchi & Saito, 2017), share similar transcription profiles with  $T_{EMRA}$  (defined as  $CD3^+CD4^+CD45RA^+CCR7^-$  cells), which exhibit the cytotoxic function of  $CD8^+$  T lymphocytes and NK cells (Patil *et al.*, 2018). Gene set enrichment analysis (GSEA) of  $CD4^+$  ITNKs shows that the “natural killer cell-mediated cytotoxicity” gene set was enriched in *BCL11B*-, *MTA2*-, *MBD2*-, and *CHD4*-deficient  $CD4^+$  ITNKs (Fig EV1E).

Of note, the PCA analysis shows that the expression profiles of *MTA2*-, *MBD2*-, and *CHD4*-deficient ITNKs were similar but different from those of *BCL11B*-deficient ITNKs (Fig 2A and

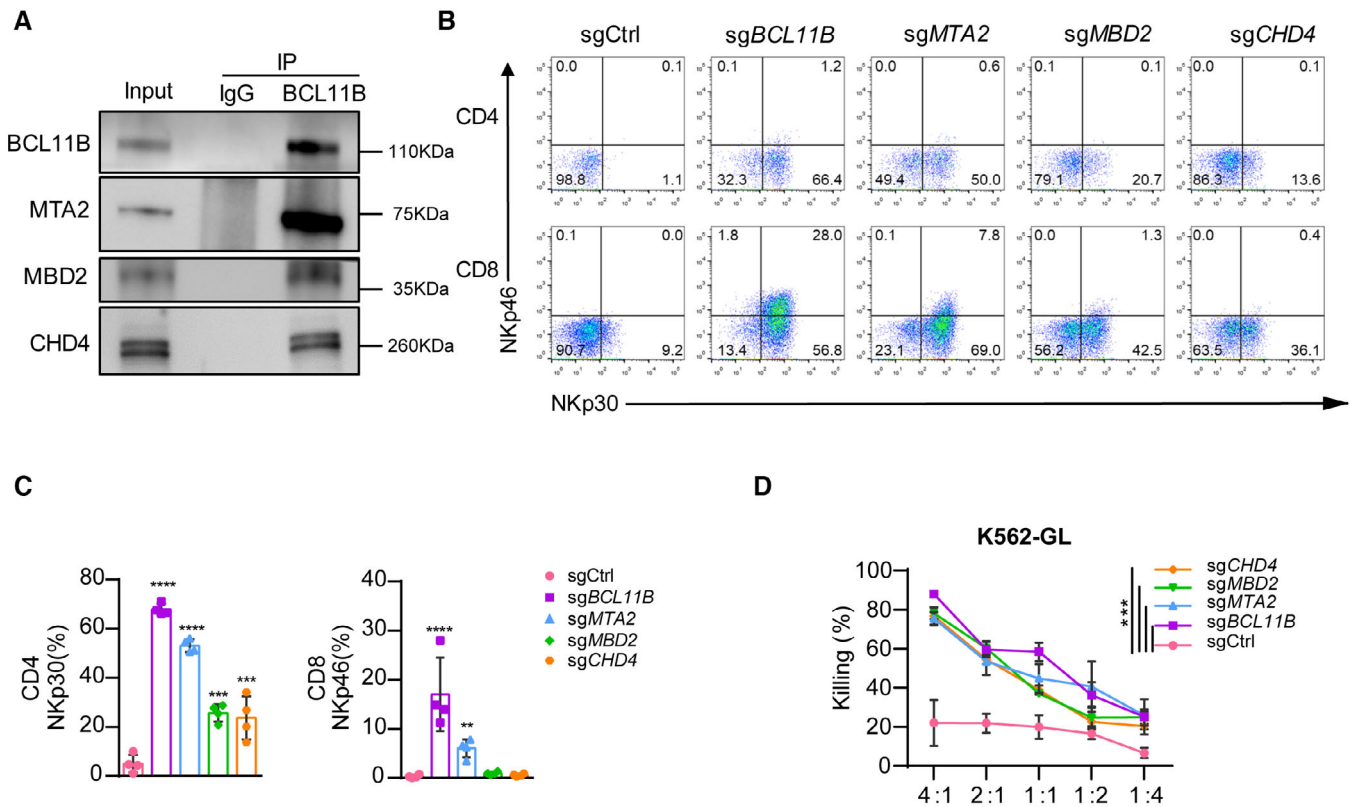


**Figure 1. Deletion of subunits of the NuRD complex reprograms human T cells into iTNks.**

**A** Immunoprecipitation of the nuclear extract of peripheral blood mononuclear cells (PBMC)-derived T cells with anti-BCL11B antibodies and western blot analysis with antibodies against the NuRD components MBD2, MTA2, and CHD4.

**B** Human T cells from PBMC were electroporated with sgCtrl, sgBCL11B, sgMBD2, sgMTA2, or sgCHD4 and Cas9 protein after activation with CD3/CD28 antibodies for 36 h. Those T cells were cultured in T cell culture medium containing rh-IL2 (300 U/ml) for 10 days. Representative flow cytometric detection of NKp30 and NKp46 expression in PBMC-derived T cells transduced with sgCtrl, sgBCL11B, sgMBD2, sgMTA2, or sgCHD4. The data shown is representative of four individual healthy donors.

**C** Graph summarizing the percentages of NKp30<sup>+</sup> in CD4 T cells and the percentages of NKp46<sup>+</sup> cells in CD8 T cells that were transduced with sgCtrl, sgBCL11B, sgMBD2, sgMTA2, or sgCHD4.

**D** After culture for 10 days, T cells in (B) were incubated with the K562-GL target cells at various E:T ratios for 24 h. Killing assays showing the percent cytotoxicity of T cells transduced with sgCtrl, sgBCL11B, sgMBD2, sgMTA2, or sgCHD4 against K562-GL cells. The data represents killing percentage of cells from a donor.

Data information: In (C and D), data are presented as mean  $\pm$  SD ( $N = 4$  individual healthy donors). \*\* $P \leq 0.01$ , \*\*\* $P \leq 0.001$  and \*\*\*\* $P \leq 0.0001$ , one-way ANOVA (C) or two-way ANOVA (D) with Tukey's multiple comparisons test.

Source data are available online for this figure.

Appendix Fig S2A and B). GO analysis suggests that upregulated genes in MTA2-, MBD2-, and CHD4-deficient iTNks were mainly involved in cellular morphogenesis pathways, while downregulated genes were enriched in immune responses and biosynthetic processes, compared with BCL11B-deficient iTNks (Appendix Fig S2C and D).

Bcl11b-repressed genes harbor high H3K27Ac peak levels when Bcl11b is absent in murine T cells (Hosokawa et al, 2018). We thus performed cleavage under targets and tagmentation (CUT&Tag) analysis to identify H3K27Ac-enriched regions and associated genes (Fig EV2A and B, Dataset EV1). We found that global H3K27 acetylation (scaled to 3 kb upstream and downstream of transcriptional start sites (TSSs)) was markedly increased in sgBCL11B-, sgMBD2-, and sgCHD4-transduced CD8<sup>+</sup> T cells as compared to CD8<sup>+</sup> sgCtrl-transduced T cells (Fig EV2C). In particular, we found that H3K27Ac binding peaks were enriched at TSSs and putative

enhancer elements sites of T-cell-activation and NK-cell-mediated immunity gene sets, including ZNF683 and ID2 in sgBCL11B- and sgCHD4-transduced CD8<sup>+</sup> T cells, as compared to CD8<sup>+</sup> sgCtrl-transduced T cells (Figs 2D and EV2D and E), which is consistent with GO enrichment of RNA-seq (Fig EV1C and D). To identify binding sites of BCL11B and CHD4 in human primary CD8<sup>+</sup> T cells, we also performed CUT&Tag analysis. We found that their binding sites overlapped with H3K27Ac binding sites at TSSs and putative enhancer element sites of ZNF683 and ID2 in primary human CD8<sup>+</sup> T cells (Figs 2D and EV2A and B). These results were in line with their derepressed expression (Fig 2B and C). In addition, BCL11B binding peaks were enriched at the loci of identified genes, including NK-cell-associated genes (ID2, IL2RB, NCR1, NCR3, and GZMB), AP-1 family member genes (JUN and JUNB), and metabolism-related genes (OPA1 and ACO2) (Fig 2E). To investigate the roles of these BCL11B-repressed genes during reprogramming of T cells into

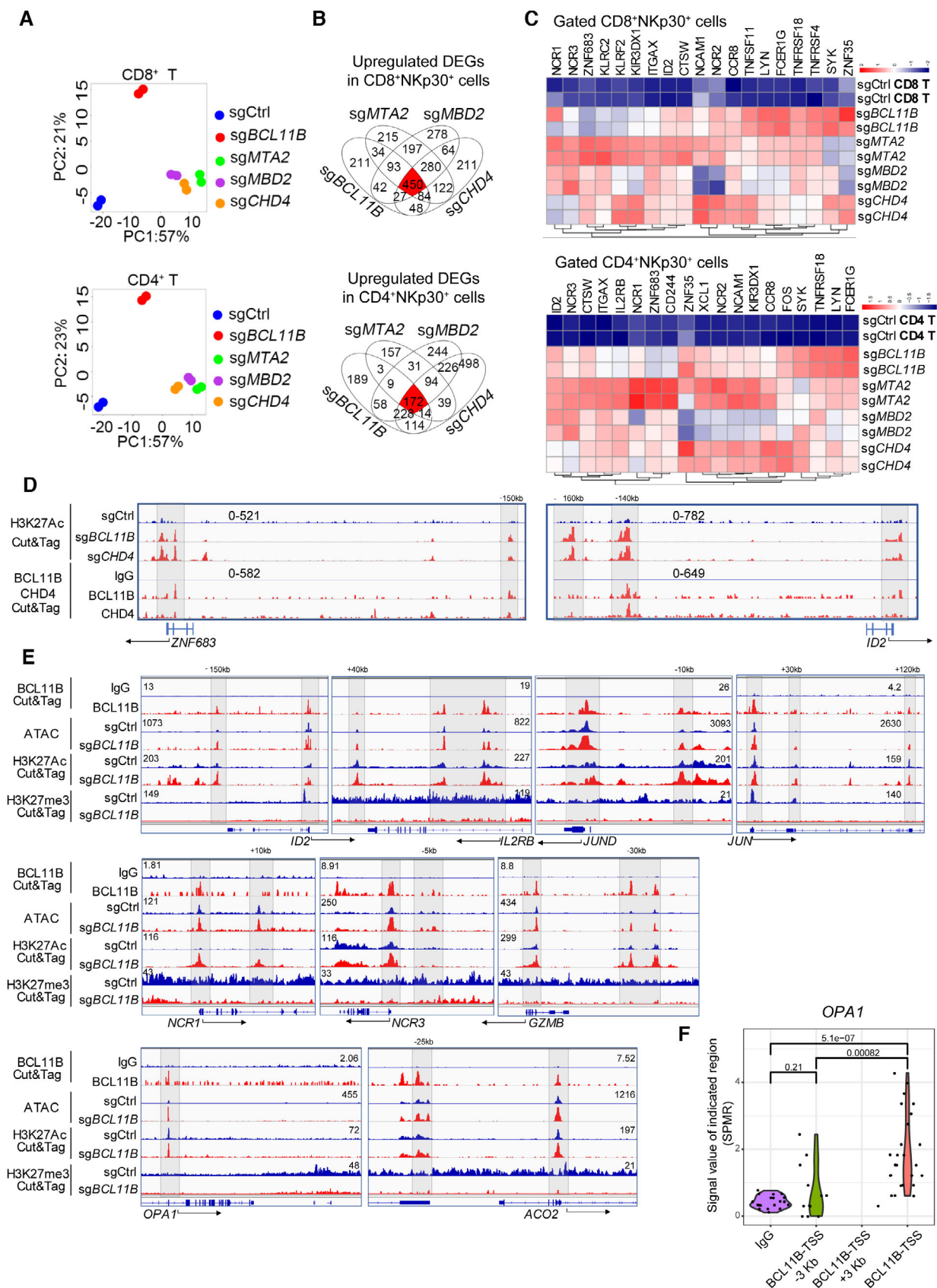


Figure 2.

**Figure 2. BCL11B associates with the NuRD complex to repress the expression of NK-cell-associated genes in human T cells.**

- A PBMC-derived T cells from two healthy donors were transduced with sgCtrl, *sgBCL11B*, *sgMTA2*, *sgMBD2*, or *sgCHD4* and cultured for 10 days. CD8<sup>+</sup>NKp30<sup>+</sup> and CD4<sup>+</sup>NKp30<sup>+</sup> cells (purity > 90%) were enriched from PBMC-derived T cells transduced with *sgBCL11B*-, *sgMTA2*-, *sgMBD2*-, and *sgCHD4*-transduced T cells, compared to CD8<sup>+</sup> and CD4<sup>+</sup> sgCtrl-transduced T cells. CD4 and CD8 T cell subsets were enriched from T cells transduced with sgCtrl. Principal component analysis (PCA) was used to evaluate the similarities in the global gene expression profiles of the listed populations.
- B Venn diagrams for the number of upregulated differentially expressed genes (DEGs) in (A) overlapping among CD8<sup>+</sup>NKp30<sup>+</sup> (450 genes) and CD4<sup>+</sup>NKp30<sup>+</sup> (172 genes) subsets from *sgBCL11B*-, *sgMTA2*-, *sgMBD2*-, and *sgCHD4*-transduced T cells, compared to CD8<sup>+</sup> and CD4<sup>+</sup> sgCtrl-transduced T cells.
- C Heatmap of the overlapping upregulated DEGs from (B).
- D PBMC-derived CD8<sup>+</sup> T cells transduced with sgCtrl, *sgBCL11B*-, and *sgCHD4* were cultured for 10 days *in vitro* before CUT&Tag experiments. Selected genome views for the H3K27Ac CUT&Tag data for *sgBCL11B*- and *sgCHD4*-transduced CD8<sup>+</sup>NKp46<sup>+</sup> cells. H3K27Ac peak data for listed NK-cell-associated genes in the indicated T cells. The data are representative of two individual healthy donors. CUT&Tag analysis of the binding of CHD4 to the loci of these genes in CD8<sup>+</sup> T cells. IgG antibodies were used as a blank control.
- E PBMC-derived T cells transduced with sgCtrl and *sgBCL11B* were cultured for 10 days *in vitro*. T cells were harvested and extracted DNA fragments marked by BCL11B antibody; sgCtrl-transduced T cells and *sgBCL11B*-transduced T cells (CD3<sup>+</sup>NKp46<sup>+</sup>) were harvested and extracted DNA fragments marked by H3K27Ac antibody and H3K27me3 antibody for CUT&Tag sequencing, respectively. These sgCtrl-transduced T cells and *sgBCL11B*-transduced T cells (CD3<sup>+</sup>NKp46<sup>+</sup>) were also lysed to extract nuclei for ATAC-seq profile. Selected genome views for the BCL11B, H3K27Ac CUT&Tag, and ATAC-seq data of T cells. CUT&Tag analysis of the binding of BCL11B to the loci of NK-related genes, AP-1, and metabolism-related genes in T cells. IgG antibodies were used as a blank control. ATAC-seq data of sgCtrl T cells and corresponding *sgBCL11B* T cells are shown in views of the indicated gene loci. H3K27Ac and H3K27me3 peak data of sgCtrl T cells and corresponding *sgBCL11B* T cells are shown in views of the indicated gene loci. The data are representative of two individual healthy donors.
- F Violin plot of the distribution of BCL11B binding peaks spanning 3 kb upstream to downstream of the TSS region of the *OPA1* gene (BCL11B CUT&Tag data from (E)). SPMR: signal per million reads.

Data information: In (F), the points represent the windows with signal values in the CUT&Tag data ( $N = 10\text{--}25$  signal values per region). We extracted the signal values from the bedgraph file generated by MACS2, and used two-tailed unpaired Student's *t*-test to evaluate the significant differences between the data. Source data are available online for this figure.

ITNKs, we ablated ID2 or JUND in combination with BCL11B in T cells and found that loss of ID2 or JUND significantly reduced the percentages of CD8<sup>+</sup>NKp46<sup>+</sup> and CD4<sup>+</sup>NKp30<sup>+</sup> cells in BCL11B-deficient T cells (Appendix Fig S2E).

To further reveal the state of chromatin, we performed transposase-accessible chromatin with sequencing (ATAC-seq) (Fig EV2A and B, Dataset EV1). The results showed that the loci of these genes overlapped with the binding sites of BCL11B and were more accessible in *sgBCL11B*-transduced T cells than in sgCtrl-transduced T cells (Fig 2E). Moreover, these loci exhibited an increase in active H3K27Ac modification and a decrease in H3K27me3 modification in *sgBCL11B*-transduced T cells as compared with sgCtrl-transduced T cells (Fig 2E).

Thus, these results were consistent with the RNA-seq data and show that BCL11B directly represses NK-cell-associated transcriptional signatures in cooperation with the NuRD complex in human T cells.

**ITNKs contain fused mitochondria with enhanced metabolic function**

We noted an elevated enrichment of metabolic gene signatures in ITNKs derived from both BCL11B- and NuRD-subunit-deficient T cells (Fig EV1A and B). We also found that H3K27Ac binding peaks increased at gene set associated with oxidative phosphorylation (Fig EV2F). In addition to NK-cell-associated genes, BCL11B also bound to the promoter region of *OPA1* (Fig 2E). To identify more potential BCL11B binding sites at nearby regions of the *OPA1* locus, we analyzed the peak from 3 kb upstream to downstream of the TSS region and found the BCL11B peaks were only significantly enriched at the TSS of *OPA1* but not at other regions (Fig 2F, Dataset EV1). We also performed a BCL11B CUT&Tag-qPCR assay and demonstrated that BCL11B indeed binds to the TSS region of *OPA1* but not the nearby control regions (Figs 3A and EV3A). Moreover, the binding site of BCL11B in the *OPA1* locus became more

**Figure 3. ITNKs contain fused mitochondria with enhanced metabolic function.**

- A Quantifying the fold enrichment of *OPA1* at different binding sites of BCL11B using CUT&Tag-qPCR.
- B Relative mRNA levels of *OPA1* in samples of human T cells, ITNKs (CD3<sup>+</sup>NKp46<sup>+</sup>), and NK cells (CD3<sup>-</sup>CD56<sup>+</sup>) based on quantitative RT-PCR.
- C Western blot analysis of mitochondrial fusion protein OPA1 levels in samples of human T cells, ITNKs (CD3<sup>+</sup>NKp46<sup>+</sup>), and NK cells (CD3<sup>-</sup>CD56<sup>+</sup>). Graph summarizing the relative protein levels of OPA1, including the long-form OPA1 (L-OPA1) and the short-form OPA1 (S-OPA1), in ITNKs compared to T cells.
- D Western blot analysis of OPA1 protein levels in ITNKs that were derived from T cells transduced with *sgBCL11B*, *sgMTA2*, *sgMBD2*, or *sgCHD4* and sgCtrl-transduced T cells.
- E Transmission electron micrograph of purified T, ITNK, and NK cells from Appendix Fig S3C. ITNKs had a low nucleocytoplasmic ratio compared to T cells. 1, nucleus; 2, mitochondria. Scale bar, 2  $\mu\text{m}$  (top) and 500 nm (bottom).
- F Confocal microscopy images showing purified T cells, ITNKs, and NK cells in which the mitochondria (MitoTracker; red) and nuclei (Hoechst; blue) are stained. Scale bars: 5  $\mu\text{m}$ . Each dot represents the mean relative length of the mitochondria in a sample.
- G ITNKs, T cells, and NK cells derived from the same donors who provided PBMCs were cultured for 10 days without activation or priming before assaying, and cell metabolism was analyzed. OXPHOS (OCR: O<sub>2</sub> consumption rate) assays were performed in real-time after injection of oligomycin (2  $\mu\text{M}$ ), FCCP (1  $\mu\text{M}$ ), and antimycin A (1  $\mu\text{M}$ ) plus rotenone (1  $\mu\text{M}$ ) as indicated.

Data information: In (A–G), data are presented as mean  $\pm$  SD,  $N = 3$  (B–G) or  $N = 4$  (A) individual healthy donors.  $N = 20$  (E) and  $N = 25$  (F) mitochondria per replicate. \* $P \leq 0.05$ , \*\* $P \leq 0.01$ , \*\*\* $P \leq 0.001$  and \*\*\*\* $P \leq 0.0001$ , two-tailed paired Student's *t*-test (B–D), one-way ANOVA with Tukey's multiple comparisons test (E–G) or two-way ANOVA with Sidak's multiple comparisons test (A). Source data are available online for this figure.

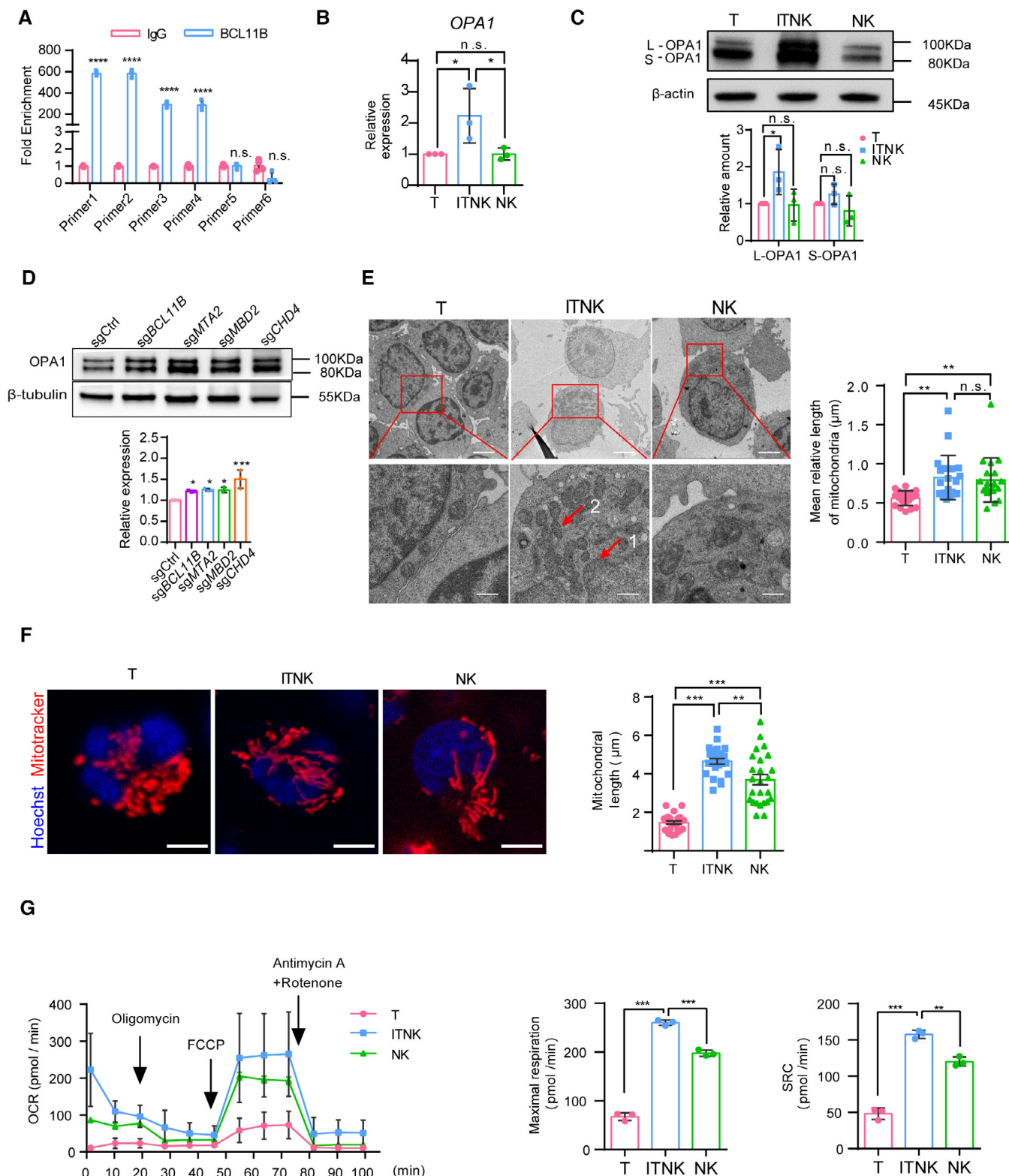


Figure 3.

accessible with increased levels of active H3K27Ac modification in human T cells upon BCL11B ablation (Fig 2E). Consistently, we found that the OPA1 transcription was upregulated in ITNKs,

compared to T cells from the re-analysis of the bulk RNA-seq data from our previous study (Jiang *et al.*, 2022; Fig EV3B). Quantitative real-time polymerase chain reaction (qPCR) also showed that the

expression of *OPA1* was derepressed in ITNKs upon BCL11B ablation, as compared with T cells (Figs 3B and EV3C). These results suggest that the expression of *OPA1*, which promotes mitochondrial fusion (Youle & van der Bliek, 2012; Buck et al, 2016), is directly repressed by BCL11B.

We next measured the levels of mitochondrial dynamics-related proteins and found that both the long- and short-form of the mitochondrial fusion protein *OPA1* were significantly upregulated in BCL11B-deficient T cells as compared to normal T cells, in line with BCL11B ablation (Figs 3C and EV3D). In particular, the ratio of the long-form *OPA1* to its short-form was increased, which promotes mitochondrial inner-membrane fusion (Fig 3C; Del Dotto et al, 2017; Ge et al, 2020). The expression of other mitochondrial dynamics-related proteins, including MFN1, MFN2, Drp1, and Drp1<sup>ps616</sup>, was unchanged between T cells and ITNKs (Fig EV3E). However, the Drp1<sup>ps616</sup> protein was significantly decreased in NK cells (Fig EV3E). Like BCL11B-deficient ITNKs, MTA2-, MBD2-, and CHD4-deficient ITNKs also showed upregulation of *OPA1* protein levels as compared to sgCtrl-transduced T cells (Fig 3D).

As *OPA1* regulates mitochondrial dynamics (Buck et al, 2016), we purified ITNKs (CD3<sup>+</sup>NKp46<sup>+</sup>) that were derived from BCL11B-deficient T cells and compared their mitochondrial morphology to that of T cells (CD3<sup>+</sup>NKp30<sup>-</sup>) and NK cells (CD3<sup>-</sup>CD56<sup>+</sup>) from the same normal donors by transmission electron microscopy (TEM) (Fig EV3F). ITNK and NK cells mostly harbor large and tubular mitochondria, while T cells had small and dispersed mitochondria (Fig 3E). In addition, we observed that ITNKs exhibited elongated and fused tubular mitochondria using confocal laser scanning microscopy (CLSM) (Fig 3F). To investigate the effects of different splice isoforms of *OPA1* on mitochondrial fusion in T cells, we overexpressed two long *OPA1* isoforms (isoform 1, isoform 1 with mutation at the S1 cleavage site ( $\Delta$ S1 mutation)) and a short isoform of *OPA1* (isoform 5) in primary human T cells. Isoform 1 functions as the fusion-active species, giving rise to long forms of *OPA1* that can be cleaved into short forms. In contrast, isoform 1  $\Delta$ S1 produces an uncleavable isoform 1 (Ishihara et al, 2006; Song et al, 2007; Del Dotto et al, 2017). Conversely, isoform 5 produces short forms of *OPA1* with little fusion activity (Ishihara et al, 2006; Song et al, 2007; Fig EV3G). In line with previous studies (Ehse et al, 2009), the expression of both long isoforms resulted in the tubulation of mitochondria, while the *OPA1* isoform 5 overexpression did not promote mitochondrial elongation (Fig EV3H). Furthermore, we induced an upregulation of *OPA1* protein in human T cells with M1 treatment that promotes mitochondrial fusion (Wang et al, 2012; Ding et al, 2020) and found that M1-treated T cells exhibited elongated mitochondria (Fig EV3I and J).

We then evaluated the mitochondrial morphology in different subpopulations of T cells and ITNKs. CD8<sup>+</sup> T cells exhibited predominantly punctate mitochondria compared to CD4<sup>+</sup> T cells (Fig EV4A and B). However, both CD4<sup>+</sup> ITNKs and CD8<sup>+</sup> ITNKs possessed similar elongated tubular mitochondria (Fig EV4A and B). Moreover, ITNKs derived from T cells by ablating NuRD subunits also contained elongated tubular mitochondria (Fig EV4C). These data suggest that *OPA1* expression could induce mitochondrial elongation in human T cells as seen in BCL11B-deficient and NuRD-subunit-deficient ITNKs.

As tubular mitochondria exhibit increased OXPHOS (Zheng et al, 2019), we examined the metabolic output of BCL11B-deficient

ITNKs and found that the oxygen consumption rate (OCR), which is an indicator of OXPHOS (Zheng et al, 2019), was higher in ITNKs than in T or NK cells (Fig 3G). In addition, the maximal respiration and mitochondrial spare respiratory capacity (SRC) measured after the addition of carbonyl cyanide-4-(trifluoromethoxy) phenylhydrazone (FCCP) were significantly increased in ITNKs as compared with T and NK cells (Fig 3G). These results suggest that BCL11B ablation upregulates the oxidative metabolism in ITNKs. CD4<sup>+</sup> and CD8<sup>+</sup> subsets of BCL11B-deficient ITNKs had significantly increased mitochondrial mass (as measured by MitoTracker green staining) (Fig EV4D) and mitochondrial membrane potential, as evaluated by staining with tetramethylrhodamine methyl ester (TMRM), as compared to CD4<sup>+</sup> and CD8<sup>+</sup> T cells, respectively (Fig EV4E). Moreover, the levels of reactive oxygen species (ROS) in these CD4<sup>+</sup> and CD8<sup>+</sup> ITNKs were lower than those in CD4<sup>+</sup> and CD8<sup>+</sup> T cells, respectively (Fig EV4F). Taken together, these results suggest that ITNKs exhibit fused mitochondria with augmented metabolic function.

### OPA1-mediated mitochondrial fusion facilitates the reprogramming of ITNKs and their cytotoxicity

To determine whether *OPA1*-mediated mitochondrial fusion was essential for reprogramming T cells into ITNKs, we ablated *OPA1* and BCL11B in T cells with the CRISPR/Cas9 technology (Appendix Fig S3A). In line with previous reports (Buck et al, 2016), mitochondria in sg*OPA1*-transduced T cells and those in BCL11B and *OPA1* double-knockout T cells were fragmented (Fig 4A). In addition, the percentages of CD4<sup>+</sup> ITNKs (CD4<sup>+</sup>NKp30<sup>+</sup>) and CD8<sup>+</sup> ITNKs (CD8<sup>+</sup>NKp46<sup>+</sup>) with BCL11B and *OPA1* double knockout in T cells were significantly decreased as compared to those in BCL11B-deficient T cells (Fig 4B). These results suggest that mitochondrial fusion facilitates the reprogramming of T cells into ITNKs upon BCL11B loss.

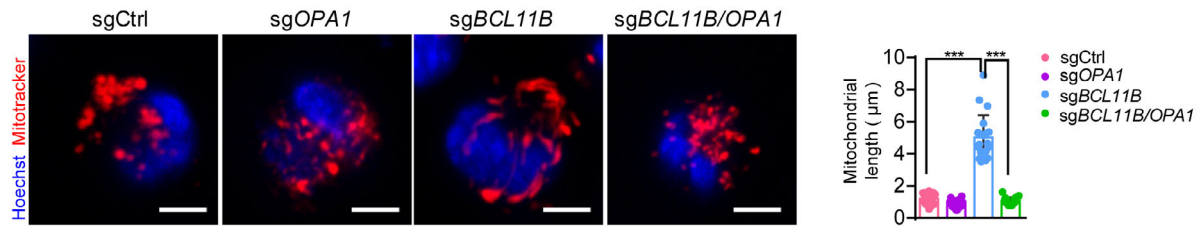
Carbonyl cyanide m-chlorophenylhydrazone (CCCP), a mitochondrial electron transport chain uncoupler, can affect *OPA1* stability and induce mitochondrial fission (Gripic et al, 2007). Indeed, we found that CCCP treatment resulted in *OPA1* cleavage of the long form into the short form in ITNKs and induced mitochondrial fission (Appendix Fig S3B and C). In addition, the OCR was significantly decreased in the CCCP-treated ITNKs, in line with mitochondrial spare respiratory capacity (Appendix Fig S3D). Like *OPA1* ablation, the CCCP treatment also decreased NKp30 and NKp46 expression in BCL11B-deficient T cells (Fig 4C). These results suggest that ablating *OPA1* to disrupt mitochondrial fusion impairs the reprogramming of T cells into ITNKs.

Since mitochondrial fusion enhances the antitumor activity of NK cells (Zheng et al, 2019), we investigated whether it was the same case for ITNKs by inhibiting mitochondrial fusion in ITNKs via CCCP treatment. The cytotoxicity of ITNKs against K562 cells was compromised upon CCCP treatment (Fig 4D). In addition, CCCP-treated ITNKs secreted less IFN $\gamma$ , granzyme B, and GM-CSF in coculture with K562 cells than untreated ITNKs (Fig 4E). These results demonstrate that *OPA1* inhibition reduces the antitumor activity of ITNKs.

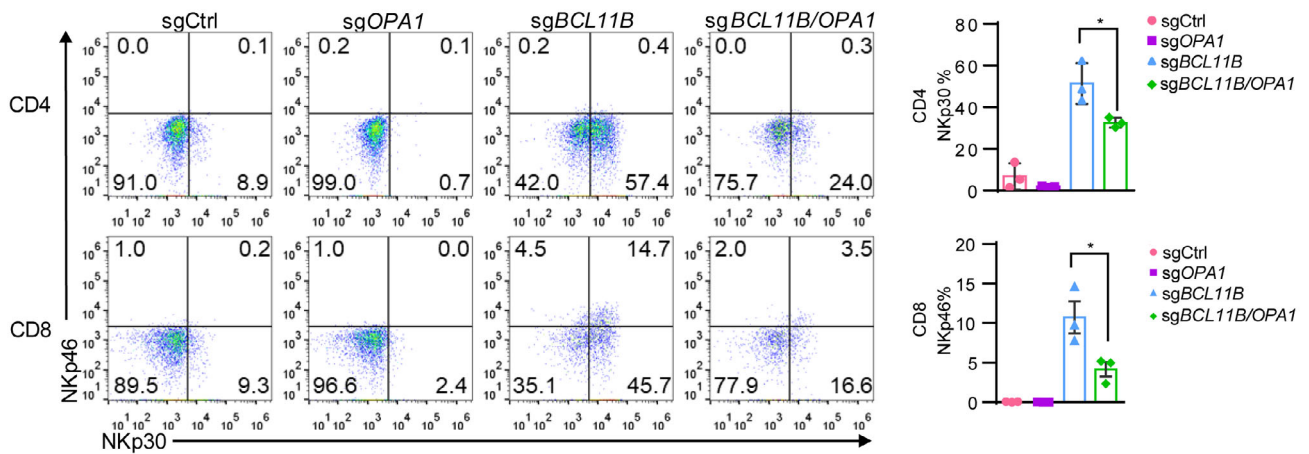
### Acetyl-CoA augments the expression of NK-cell-associated genes and antitumor effects in ITNKs by regulating histone acetylation

Mitochondrial fusion favors OXPHOS metabolism in T cells (Buck et al, 2016). Our previous data showed that the tricarboxylic acid

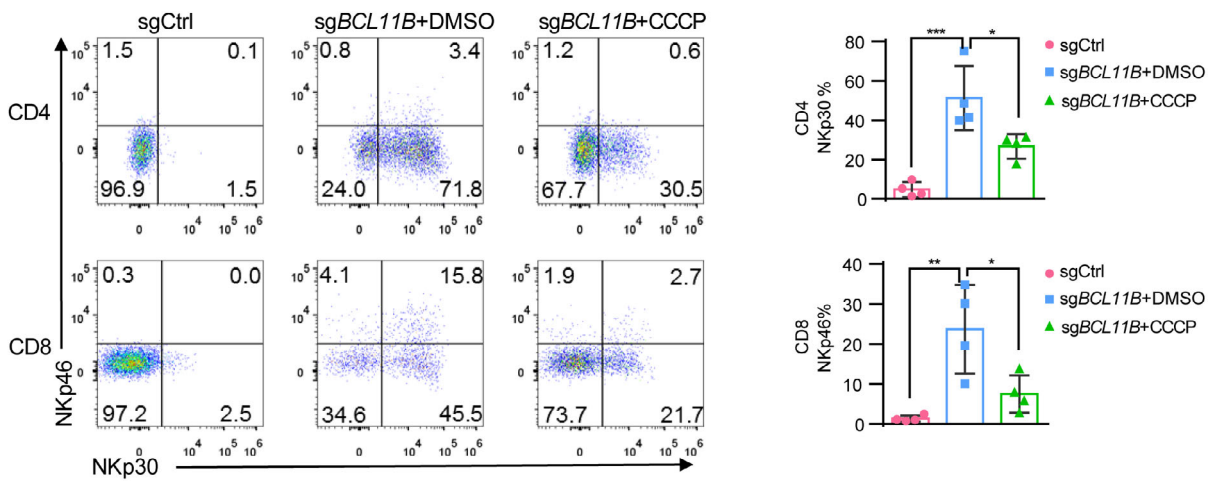
**A**



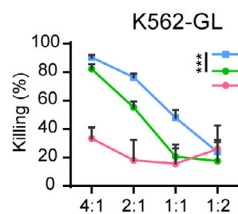
**B**



**C**



**D**



**E**

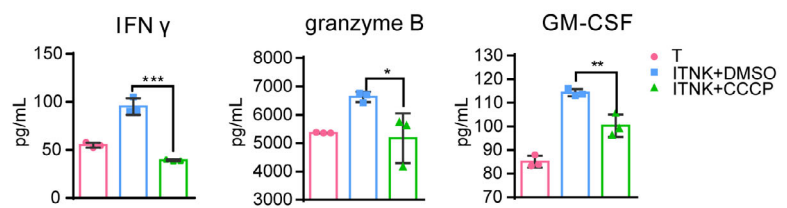


Figure 4.



**Figure 4. OPA1-mediated mitochondrial fusion facilitates the reprogramming of ITNKs and their cytotoxicity.**

- A Confocal microscopy images showing T cells transduced with sgCtrl, sgOPA1, sgBCL11B, or sgBCL11B/OPA1 in which the mitochondria (MitoTracker, red) and nuclei (Hoechst; blue) are stained. Scale bars: 5  $\mu$ m. Mean lengths of the 20 mitochondria per replicate, as analyzed by confocal microscopy, are shown.
- B Representative flow cytometric analysis of NKp30 and NKp46 expression in T cells transduced with sgCtrl, sgOPA1, sgBCL11B, or the combination of sgBCL11B and sgOPA1. A graph summarizing the percentages of NKp30<sup>+</sup> cells in CD4<sup>+</sup> T cells and percentages of NKp46<sup>+</sup> cells in CD8<sup>+</sup> T cells transduced with sgCtrl, sgOPA1, sgBCL11B, or the combination of sgBCL11B and sgOPA1 is in the right panel.
- C CCCP (5  $\mu$ M, mitochondrial fission inducer) was added to a culture of sgBCL11B-transduced human T cells derived from PBMCs 24 h after electroporation. Ten days later, the T cells were subjected to FACS analysis. A graph summarizing the percentages of NKp30<sup>+</sup> and NKp46<sup>+</sup> cells in CD4<sup>+</sup> and CD8<sup>+</sup> T cells transduced with sgCtrl, sgBCL11B, or sgBCL11B and treated with CCCP is shown in the right panel.
- D Killing assays showing the percent cytotoxicity of T cells, ITNKs, and ITNKs treated with CCCP from (C) against K562 cells. The data represents killing percentage of cells from a donor.
- E Cytokine secretion profiles of T cells, ITNKs, and ITNKs treated with CCCP and cocultured with K562 cells. T cells, ITNKs, and ITNKs treated with CCCP from (C) were incubated with K562 cells at an E:T ratio of 1:1 for 24 h. The supernatants were then harvested, and the concentrations of the indicated cytokines were measured by a multiplex immunoassay. The data represents the concentrations of the indicated cytokines from (D).

Data information: In (A, B, D and E), data are presented as mean  $\pm$  SD,  $N = 3$  or  $N = 4$  (C) individual healthy donors. \* $P \leq 0.05$ , \*\* $P \leq 0.01$  and \*\*\* $P \leq 0.001$ , two-tailed paired Student's *t*-test (B–D), one-way ANOVA (A–C) or two-way ANOVA (D and E) with Tukey's multiple comparisons test. Source data are available online for this figure.

(TCA) cycle and FAO process-related gene were upregulated in ITNKs (Jiang *et al*, 2022; Fig EV3B). Consistently, a recent publication demonstrates that Th17 cells have fused mitochondria and require OPA1 for its control of the TCA cycle to regulate effector programs (Baixauli *et al*, 2022), which implies that the increase in OPA1 may elevate TCA metabolism through mitochondrial fusion in ITNKs. Metabolites act as a source for biomacromolecule synthesis in cells and provide key substrates for epigenetic modification (Matalainen *et al*, 2017; Wu *et al*, 2022). Acetyl-CoA and  $\alpha$ -KG are key metabolites in the TCA cycle and participate in the regulation of histone modification in mammalian cells (Sutendra *et al*, 2014; Pietrocola *et al*, 2015). We measured the levels of acetyl-CoA and  $\alpha$ -KG in ITNKs and found that Acetyl-CoA but not  $\alpha$ -KG were increased in ITNKs, compared to T cells (Fig EV5A and B). In addition, the loss of OPA1 decreased Acetyl-CoA levels in ITNKs (Fig 5A). Moreover, acetate, a precursor of acetyl-CoA (Zhou *et al*, 2019), increased the acetyl-CoA level in BCL11B and OPA1 double-knockout ITNKs (Fig 5A). Strikingly, acetate treatment elevated the expression of NKp30 and NKp46 in CD4<sup>+</sup> and CD8<sup>+</sup> BCL11B and OPA1 double-knockout ITNKs, respectively (Figs 5B and EV5C). Furthermore, the loss of OPA1 compromising the cytotoxicity of BCL11B-deficient ITNKs could be rescued by acetate supplementation (Fig 5C). In addition, the decreased secretion of IFN $\gamma$ , granzyme B, and GM-CSF in BCL11B-deficient ITNKs in coculture with HepG2 cells observed when OPA1 is depleted, could be reversed by acetate treatment (Fig EV5D). These results suggest that acetyl-CoA facilitates the reprogramming of ITNKs and promotes their antitumor effects.

Since levels of acetyl-CoA were increased in BCL11B-deficient T cells (Fig 5A), we measured the acetylation levels of H3K27Ac in

total histone proteins and found that the overall level of H3K27Ac was increased in BCL11B-deficient ITNKs compared to sgCtrl-transduced T cells (Fig 5D). Consistent to the acetyl-CoA level, the H3K27Ac level in BCL11B and OPA1 double-knockout ITNKs was lower than that in BCL11B-deficient ITNKs but still higher than that in sgCtrl-transduced T cells (Fig 5D). Of interest, acetate treatment augmented the level of H3K27Ac in BCL11B and OPA1 double-knockout ITNKs (Fig 5D).

In particular, chromatin immunoprecipitation coupled with quantitative PCR (ChIP-qPCR) assessment of H3K27Ac showed that H3K27Ac was enriched at the loci of NK-cell related genes, including *ZBTB16*, *NCR1*, *NCR3*, *IFNG*, *GZMB*, and *CSF2* (Louis *et al*, 2020), in sgBCL11B-transduced T cells compared to sgCtrl-transduced T cells (Fig 5E). These results were consistent with the analyses of H3K27Ac CUT&Tag and ATAC-seq in BCL11B-deficient ITNKs and sgCtrl-transduced T cells (Fig 2E). There was a decreased H3K27Ac level at the loci of these of NK-cell-associated genes in BCL11B and OPA1 double-knockout ITNKs (Fig 5E). However, the decrease in H3K27Ac at these loci was restored by acetate treatment in BCL11B and OPA1 double-knockout ITNKs (Fig 5E). Consistently, the mRNA levels of the NK-cell-related genes varied and were correlated to the H3K27Ac levels at their loci in different types of ITNKs with or without acetate treatment, while the expression of housekeeping genes (*EEF2*, *B2M*, *MYH9*, and *TUBB*) did not (Fig EV5E). Taken together, these results suggest that acetyl-CoA promotes the expression of NK-cell-associated genes, cytotoxic cytokine secretion, and ITNK cytotoxicity through regulating H3K27Ac modifications.

To further confirm whether T cells acquire the NK-cell potential through a metabolic-epigenetic axis, we measured the levels of

**Figure 5. Acetyl-CoA augments the expression of NK-cell-associated genes and antitumor effects in ITNKs by regulating histone acetylation.**

- A T cells transduced with sgCtrl and ITNKs that were reprogrammed from T cells transduced with sgBCL11B or the combination of sgBCL11B and sgOPA1 and were treated with or without acetate (20 mM) 24 h after electroporation. Relative acetyl-CoA levels of those T cells were measured on Day 10 of the cell culture.
- B Representative flow cytometry detection of NKp30 and NKp46 expression in T cells and ITNKs from (A).
- C Killing assays showing the percent cytotoxicity of T cells and ITNKs from (A) against HepG2 cells. The data represents killing percentage of cells from a donor.
- D Western blot analysis of H3K27Ac in samples of T cells and ITNKs from (A).
- E ChIP-qPCR analysis of H3K27Ac in the loci of indicated genes in T cells and ITNKs from (A).

Data information: In (A and C–E), data are presented as mean  $\pm$  SD,  $N = 3$  (C and D) or 5 (A and E) individual healthy donors. \* $P \leq 0.05$ , \*\* $P \leq 0.01$ , \*\*\* $P \leq 0.001$  and \*\*\*\* $P \leq 0.0001$ , one-way ANOVA (A) or two-way ANOVA (C) with Tukey's multiple comparisons test, two-tailed paired Student's *t*-test (D), or one-way ANOVA with Sidak's multiple comparisons test (E).

Source data are available online for this figure.

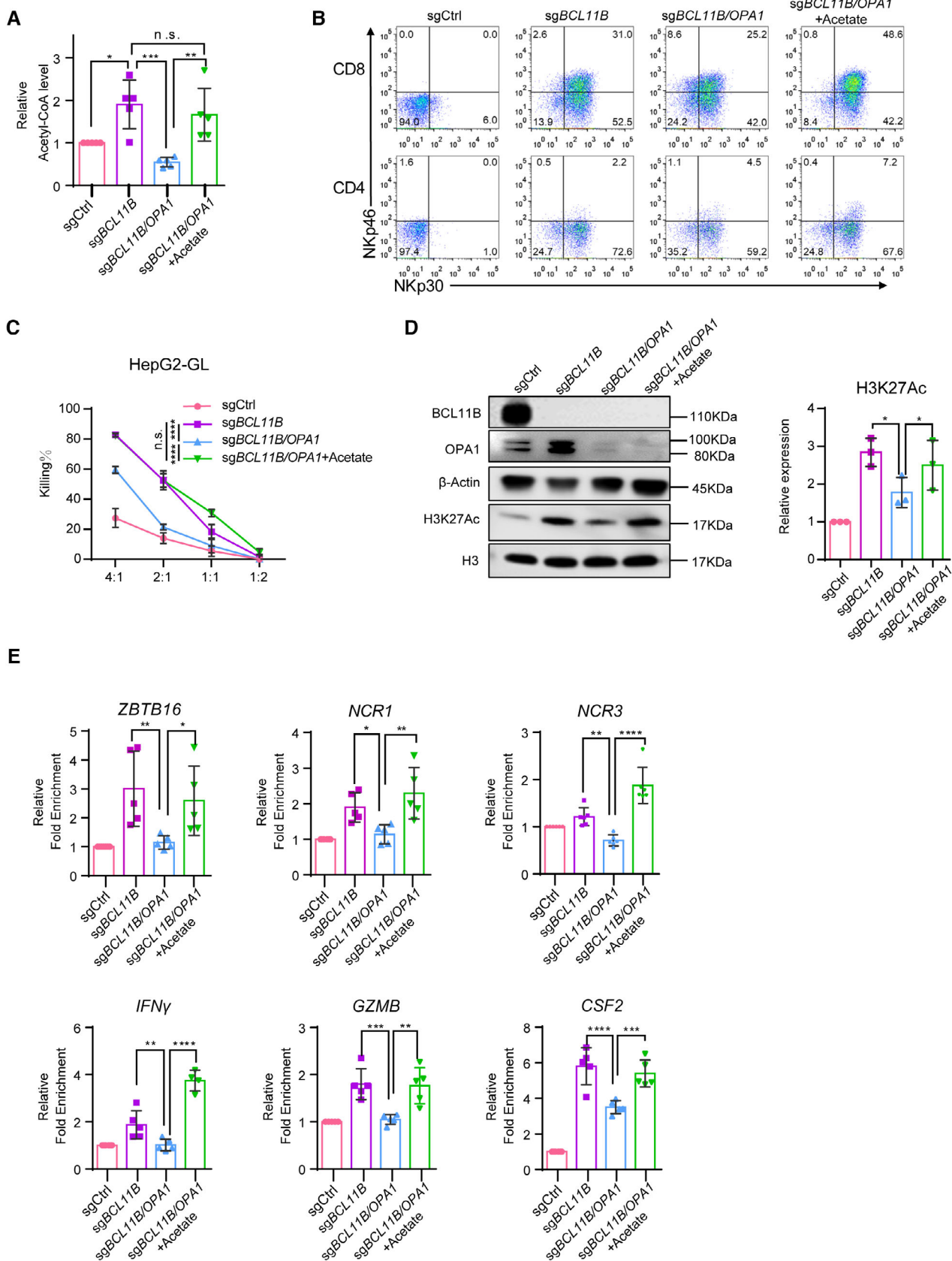


Figure 5.

OPA1 and observed the morphology of mitochondria in T cells at different time-points post-BCL11B ablation to determine the time-point when OPA1-mediated fusion occurred. We found a gradual increase of OPA1 expression following BCL11B ablation, with a significant elevation of OPA1 expression observed on Day 4 upon BCL11B loss, along with the occurrence of mitochondrial fusion (Fig 6A and B). Subsequently, we performed a mitochondrial-stress test by Seahorse on Days 2 and 4 post-BCL11B ablation at the early stage of the reprogramming and found that OCR of T cells with BCL11B ablation was significantly improved on Day 4 (Fig 6C). These results suggest that the metabolic changes occur in T cells on Day 4 upon BCL11B ablation. We then confirmed whether epigenetic changes and gaining of NK cell potential in these T cells occur on Day 4 post-BCL11B loss, by measuring the levels of H3K27Ac modification at the loci of *OPA1*, *ID2*, *ZBTB16*, and *ZNF683* and their expression. Indeed, H3K27Ac CUT&Tag-qPCR showed that H3K27Ac modification at the loci of *OPA1*, *ID2*, *ZBTB16*, and *ZNF683* was also significantly increased on Day 4 upon BCL11B ablation but not earlier (Fig 6D). In addition, RT-qPCR analysis confirmed that the expression of *ID2*, *ZBTB16*, and *ZNF683* was upregulated on Day 4 but not earlier (Fig 6E and Appendix Fig S4A and B). Taken together, these results show that the metabolic and epigenetic changes alongside the upregulation of mRNA and protein levels of NK-cell markers all initiate on Day 4 upon BCL11B ablation, suggesting that metabolic-epigenetic changes at least partially contribute to the acquisition of NK cell identity in BCL11B-deficient T cells.

## Discussion

BCL11B maintains T-cell identity, as its loss induces T cells to reprogram into NK-like cells (Li et al, 2010b; Jiang et al, 2022). In murine T cells and human T cells, BCL11B physically associates with subunits of the NuRD complex (Cismasiu et al, 2005; Hosokawa et al, 2018). Hosokawa et al (2018) reported that ablation of Mta1 and Mta2 blocks T-cell differentiation and affects the transcription of Bcl11b-regulated genes in murine T-cell progenitors. However, whether the NuRD complex guards T-cell fate remains unknown. Here, for the first time, we demonstrate that human T cells were reprogrammed into NK-like cells by deletion of MTA2, MBD2, or CHD4, suggesting that BCL11B associates with the NuRD complex to impede the NK-cell program in an evolutionarily conserved manner (Fig 1B). Previous studies show that BCL11B interacts with the NuRD complex via its subunits MTA1/2/3 (Cismasiu et al, 2005; Dubuissez et al, 2016). However, our results showed that MTA1-deficient T cells did not reprogram into NK-like cells (Appendix Fig S1B). This is probably due to the convergence of genomic occupancy sites of Mta2 and Bcl11b in T cells (Hosokawa et al, 2018). These results suggest that deletion of the MTA2 is more likely to weaken the transcriptional repression of BCL11B targeting genes, including NK-related genes.

Recent studies demonstrate that mitochondrial dynamics dictate T-cell fates via regulating metabolism in mature T cells, including T cell activation and exhaustion (Buck et al, 2016; Ron-Harel et al, 2016; Yu et al, 2020). The roles of Bcl11b during the formation of effector and memory T cells have been investigated extensively showing complexity (Zhang et al, 2010; Califano et al, 2014;

Lorentsen et al, 2018; Sidwell & Rothenberg, 2021). Nevertheless, whether Bcl11b regulates metabolism through mediating mitochondrial dynamics in T cells has not yet been elucidated. Our findings showed that BCL11B directly repressed OPA1 transcription and OPA1-mediated mitochondrial fusion facilitating ITNK reprogramming and cytotoxicity, thus revealing a potential role of BCL11B in mediating metabolic activities in T cells, besides guarding T-cell fate. Further studies are warranted to investigate whether BCL11B suppresses mitochondrial fusion via OPA1 during T-cell development and differentiation.

It is interesting to notice that NK cells expressed lower amount of the short OPA1 protein than T cells, though they had similar levels of OPA1 mRNA. This discrepancy is possibly due to the lower translation efficiency of the short form OPA1 in NK cells, or accelerated protein degradation following translation (Ehse et al, 2009). As short OPA1 promotes mitochondrial fragmentation, a lower amount of short OPA1 may result in elongated mitochondria in NK cells (Ishihara et al, 2006; Ehse et al, 2009). In addition, we found that levels of Drp1<sup>ps616</sup>, which promotes Drp1-mediated mitochondrial fission (Zheng et al, 2019; Gao et al, 2022a), were lower in NK cells than in T cells (Fig EV3E). This could also contribute to increase the length of mitochondria in NK cells.

Metabolic pathways provide not only energy but also necessary substrates for epigenetic modification to regulate gene expression (Yu et al, 2020; Fanucchi et al, 2021). We confirmed that OXPPOS was increased in T cells upon BCL11B ablation (Figs 3G and EV2F). To reveal how OPA1 impacts acetyl-CoA levels, we re-analyzed the bulk RNA-seq data of ITNKs and T cells from our previous study (Jiang et al, 2022) and found that the tricarboxylic acid (TCA) and fatty acid oxidation (FAO) processes-related genes were upregulated in ITNKs, as compared to T cells (Fig EV3B). Previous studies demonstrate that mitochondrial fusion favors TCA and FAO (Buck et al, 2016; Baixauli et al, 2022). In addition, Acetyl-CoA and  $\alpha$ -KG are key metabolites in the TCA cycle and participate in the regulation of histone modification (Shen et al, 2015; Liu et al, 2017; Morris et al, 2019). We found that the levels of Acetyl-CoA but not  $\alpha$ -KG were increased in ITNKs, compared to T cells (Fig EV5A and B). Consistently, ITNKs expressed OPA1 at higher levels than T cells (Fig 3C). Taken together, it is likely that OPA1 increases Acetyl-CoA levels through promoting mitochondrial fusion and TCA during ITNK reprogramming. Therefore, the loss of OPA1 decreased Acetyl-CoA levels in ITNKs (Fig 5A). Consistently, a recent publication demonstrates that Th17 cells have fused mitochondria and require OPA1 for its control of the TCA cycle to regulate effector programs (Baixauli et al, 2022). However, the specific source of acetyl-CoA needs to be determined by isotope-based metabolic flux analysis.

Our data showed that acetyl-CoA level was positively correlated to the expression of OPA1 in ITNKs (Fig 5A). In addition, the enrichment of H3K27Ac at the loci of NK-cell-associated genes was positively correlated to the acetyl-CoA level in ITNKs. Together, these results suggest that OPA1 facilitates the ITNK reprogramming by raising acetyl-CoA levels for acetylation of H3K27 modifications at the loci of NK-cell related genes. Current efforts are devoted to understand how acetylation of H3K27 modifications mediated by acetyl-CoA occurred specifically at the loci of NK cell-associated genes. The histone acetyltransferases (HAT), such as EP300 and GCN5, promote the expression of specific genes through regulating dynamic hyper-acetylated chromatin states and acetylation

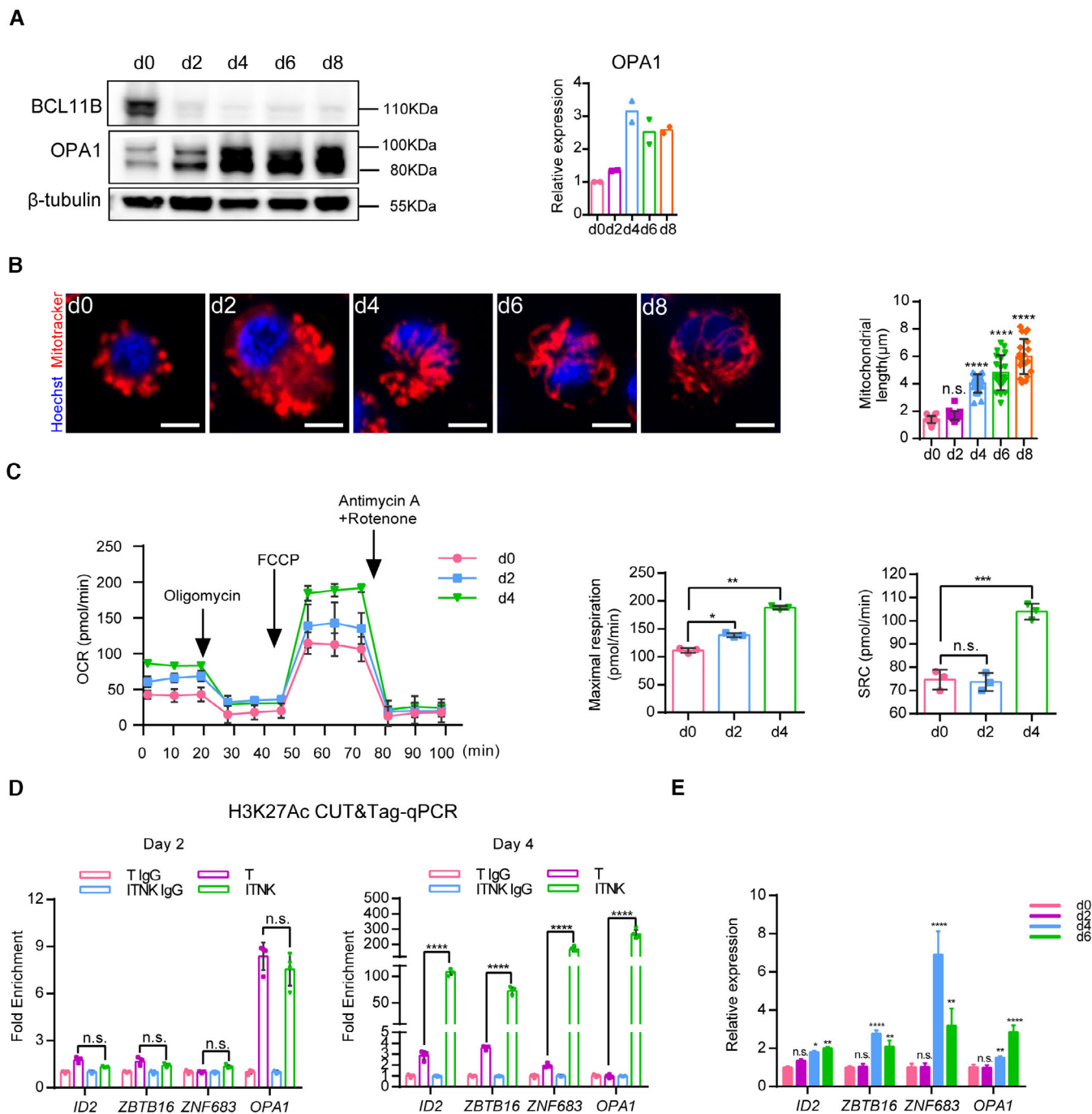


**Figure 6. ITNKs acquire the NK-cell identity through a metabolic-epigenetic axis.**

A Representative western blot analysis of BCL11B and OPA1 protein levels in ITNKs from Days 0 to 8.  
 B Representative confocal microscopy images showing ITNKs from Days 0 to 8 in the reprogramming process in which the mitochondria (MitoTracker; Red) and nuclei (Hoechst; blue) are stained. Scale bars: 5  $\mu$ m. Each dot represents the mean length of the 20 mitochondria per replicate.  
 C Mitochondrial-stress test on Days 2 and 4 of ITNKs.  
 D CUT&Tag-qPCR analysis of H3K27Ac enrichment in the promoter regions of indicated genes on Days 2 and 4 of ITNKs.  
 E Time-course analysis of NK-related transcription factors and OPA1 expression by RT-qPCR.

Data information: In (A–E), data are presented as mean  $\pm$  SD,  $N = 2$  (A and B) or 3 (C) or 4 (D and E) individual healthy donors. \* $P \leq 0.05$ , \*\* $P \leq 0.01$ , \*\*\* $P \leq 0.001$  and \*\*\*\* $P \leq 0.0001$ , one-way (C) or two-way (E) ANOVA with Dunnett’s multiple comparisons test, or two-way ANOVA with Bonferroni’s multiple comparisons test (D).

Source data are available online for this figure.

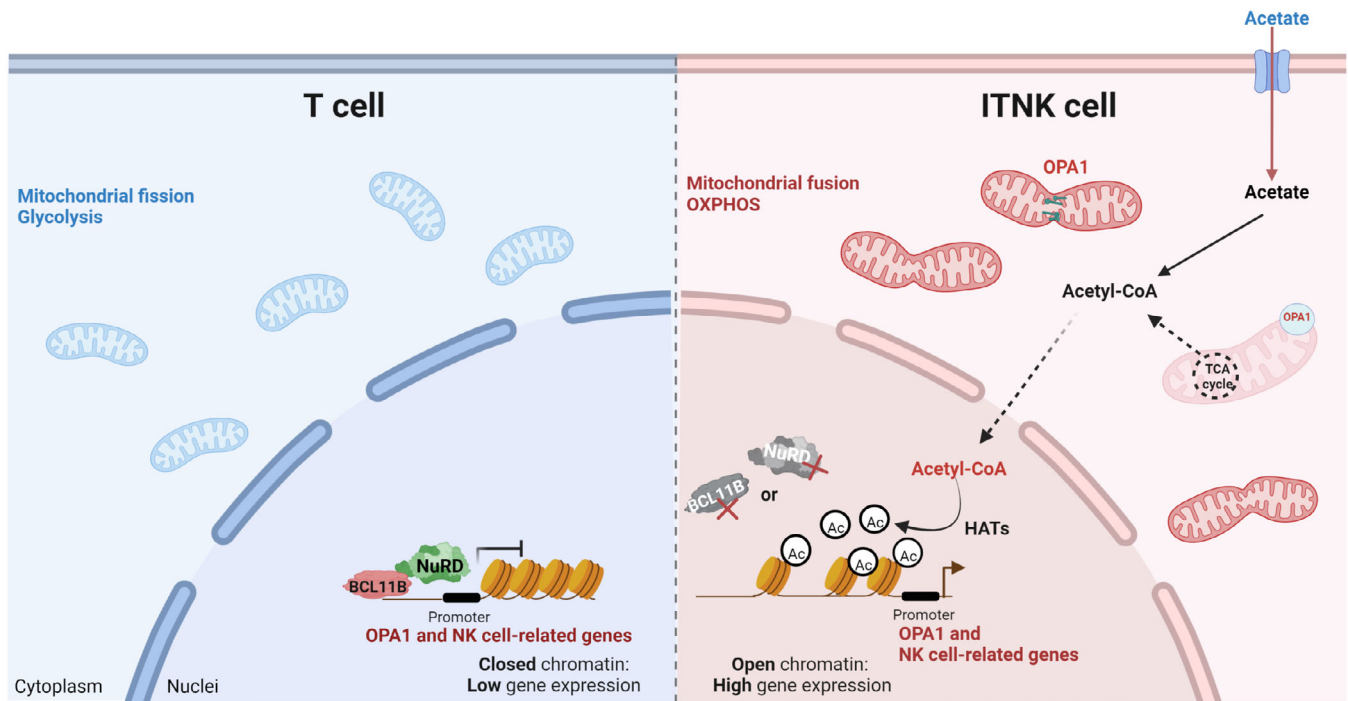


**Figure 7. The BCL11B-NuRD complex mediates mitochondrial dynamics to promote the reprogramming of T cells to ITNKs via epigenetic remodeling.** Schematic representation of the mechanism by which BCL11B and the NuRD complex inhibit the expression of OPA1 and NK-cell-associated genes in human T cells (left). OPA1-mediated mitochondrial fusion regulated by the BCL11B-NuRD complex promotes the reprogramming from T cells into ITNKs by regulating H3K27 acetylation (right). The graphics were created with [BioRender.com](https://www.biorender.com).

modifications at enhancers (Sen *et al*, 2019; Wang *et al*, 2020; Durbin *et al*, 2022). Possibly, HATs participate the upregulation of NK cell-related gene expression via inducing H3K27 acetylation modifications (Fig 7).

In summary, we investigated the functions of the NuRD complex and BCL11B in primary human T cells with loss of function studies. Our findings show that BCL11B and the NuRD complex not only directly suppress the expression of NK-cell-associated genes but also may suppress their transcription indirectly through regulating OPA1-mediated mitochondrial metabolism. Our results extend current knowledge on how mitochondrial dynamics regulate T cell fates. In addition, our work reports alternative methods to derive ITNKs, potent tumor killer cells, from T cells and provides strategies to improve the reprogramming efficiency and antitumor effects of BCL11B-deficient ITNKs.

It is important to uncover whether BCL11B suppresses mitochondrial fusion via OPA1 during T-cell development and differentiation. However, we did not address this question in this work. Further studies are warranted to investigate potential mechanisms on how BCL11B regulates mitochondrial dynamics during T cell development.

Although BCL11B protein level in NK cells was lower than that in T cells, the levels of OPA1 mRNA and protein in NK cells were similar to that in T cells, suggesting that the transcription of OPA1 may be regulated by other factors, rather than BCL11B in NK cells. Further investigation is warranted to reveal how OPA1 transcription is regulated in NK cells.

## Materials and Methods

### Isolation, transduction, and expansion of primary human T cells and NK cells

Healthy PBMC donors provided informed consent for the use of their samples for research purposes, and all procedures were approved by the Research Ethics Board of the Guangzhou Institutes of Biomedicine and Health, Chinese Academy of Sciences (GIBH, CAS). For all preclinical experiments in this study, human primary T cells were negatively selected using human T-cell negative enrichment kits (STEMCELL Technologies, Vancouver, BC, Canada) from peripheral blood mononuclear cells (PBMCs), which were isolated from healthy donors using Lymphoprep (STEMCELL Technologies, Vancouver, Canada). Subsequently, T cells were activated with 5  $\mu$ l MACS T Cell TransAct™ (130-111-160, Miltenyi Biotec, Bergisch Gladbach, Germany) at a bead:cell ratio of 1:2 and a density of  $1 \times 10^6$  cells/ml for 24 h in T551-H3 (Takara, Japan) medium supplemented with 5% heat-inactivated fetal bovine serum (FBS), 500 U/ml recombinant human IL-2, 10 mM HEPES, 2 mM glutamine, and 1% penicillin/streptomycin. NK cells were activated with the NK Cell Activation/Expansion Kit (130-094-483, Miltenyi Biotec, Germany), which contains microbeads loaded with anti-NKp46 and anti-CD2 antibodies, and were cultured in T551-H3 medium supplemented with IL-2 (500 U/ml) and 5% FBS at an initial density of  $1 \times 10^6$  cells/ml.

## Induction and expansion of ITNKs

For electroporation, on post-activation Day 1, Cas9 RNPs were prepared by incubating 20  $\mu\text{M}$  Cas9 with 20  $\mu\text{M}$  sgRNA at a 1:1 ratio in Human T-Cell Nucleofector buffer to a final concentration of 10  $\mu\text{M}$  at 37°C for 10 min (Stadtmauer *et al*, 2020). T cells were electroporated immediately with sgBCL11B RNP ( $5 \times 10^6$  T cells per reaction) using Amaxa Nucleofector 2b (Amaxa® Human T Cell Nucleofector® Kit, Lonza, Germany) with electroporation program T-023. Twelve hours after electroporation, T cells were cultured in T-cell culture medium containing rh-IL2 (500 U/ml). Subsequently, fresh medium was added every 2 days to maintain the cell density within the range of  $0.5\text{--}1 \times 10^6$  cells/ml. CD3<sup>+</sup>NKp46<sup>+</sup>/CD3<sup>+</sup>NKp30<sup>+</sup> T cells were defined as ITNKs and used in this study.

## Cell lines

Human HCC cell lines (HepG2/HepG2-GL) were maintained in Dulbecco's modified Eagle's medium (DMEM) (Gibco, Grand Island, NY, USA). Human leukemia cell lines (K562/K562-GL) were maintained in RPMI-1640 medium supplemented with 10% heat-inactivated FBS (Gibco, Grand Island, NY, USA), 10 mM HEPES, 2 mM glutamine (Gibco, Grand Island, NY, USA) and 1% penicillin/streptomycin (Gibco, Grand Island, NY, USA). All cells were cultured at 37°C in an atmosphere of 5% carbon dioxide. Cell line identity was confirmed by STR sequencing.

## Protein isolation and immunoblotting

Cells were lysed with RIPA buffer (Pierce, Rockford, Illinois, USA), and proteins were quantified using a BCA Protein Assay Kit (Pierce, Rockford, IL, USA). Samples were loaded onto a 4–20% SDS–PAGE gel, blotted onto a PVDF membrane, and sequentially probed with primary antibodies. A species-matched HRP-conjugated secondary antibody was purchased from Cell Signaling Technology (Boston, USA) and then added to detect proteins by autoradiography using an enhanced chemiluminescence kit (ECL Plus, General Electric Healthcare, Little Chalfont, UK).

## Coimmunoprecipitation (Co-IP) assay

A total of  $5 \times 10^7$  T cells were lysed in 1 ml of IP lysis buffer (150 mM KCl, 1% Triton X-100, 50 mM Tris–HCl pH 7.6, 1 mM EDTA, 10% glycerol, 1 mM phenylmethylsulfonyl fluoride (PMSF), 10 mg/l aprotinin, and 10 mg/l leupeptin), and cleared cell lysates were incubated with 10  $\mu\text{l}$  Protein A/G beads (88802) (Thermo Scientific, USA) and the appropriate antibody (5–10  $\mu\text{g}$ ) overnight at 4°C. Following incubation, the resin was washed three times with IP wash buffer (150 mM KCl, 0.1% Triton X-100, 50 mM Tris–HCl pH 7.6, 1 mM EDTA, and 1 mM PMSF), and protein samples were eluted by boiling in 1  $\times$  SDS sample buffer (30  $\mu\text{l}$ ) for western blotting analysis.

## Flow cytometry and cell sorting

Flow cytometric analysis was performed on a FACSCanto or FACS-Fortessa (BD, USA). Fluorescence-activated cell sorting (FACS) was performed on a FACS AriaII platform (BD, USA). Surface staining

for flow cytometry and cell sorting was performed by pelleting cells and resuspending them in 50  $\mu\text{l}$  of FACS buffer (2% FBS in PBS) with antibodies for 30 min at 4°C in the dark. Cells were washed once in FACS buffer before resuspension. Antibodies for cell-surface markers are shown in Table 1 and were purchased from BioLegend (San Diego, USA). The gating strategy for flow cytometry is shown in Fig EV3F.

## Transmission electron microscopy (TEM)

Cells were washed twice with phosphate-buffered saline (PBS) and then fixed with 3% glutaraldehyde. The ultrastructure of mitochondria was examined by TEM.

## Mitochondrial dynamic imaging

For mitochondrial imaging, cultured T, ITNK, and NK cells were stained with MitoTracker® Green (Yeasen, 40742ES50, China) or Deep Red FM (40743ES50, Yeasen, China) for 30 min and then stained with Hoechst 33342 (C1029, Beyotime, China) for nuclear staining for 30 min at 37°C. After washing twice with preheated culture medium, the cells were surface stained and processed for flow cytometry or confocal microscopy. Confocal laser scanning microscopy (CLSM) was carried-out on an LSM 710 NLO scanning confocal imaging workstation (Oberkochen, Germany). The length of stained mitochondria was measured using ImageJ. The mean relative length of mitochondria was obtained by measuring the length of mitochondria in each cell and statistically analyzing 20–30 cells.

## ATAC sequencing

ATAC-seq was performed as previously described (Li *et al*, 2017). In brief, a total of 50,000 cells were washed once with 50  $\mu\text{l}$  of cold PBS and suspended in 50  $\mu\text{l}$  of lysis buffer (10 mM Tris–HCl pH 7.4, 10 mM NaCl, 3 mM MgCl<sub>2</sub>, and 0.2% (v/v) IGEPAL CA-630). Suspended nuclei were then centrifuged for 10 min at 500 g at 4°C, followed by the addition of 50 ml of transposition reaction mix (25  $\mu\text{l}$  TD buffer, 2.5  $\mu\text{l}$  Tn5 transposase, and 22.5  $\mu\text{l}$  nuclease-free H<sub>2</sub>O) from the Nextera DNA Library Preparation Kit (96 samples) (FC-121-1031, Illumina, USA). Samples were then PCR amplified and incubated at 37°C for 30 min. DNA was isolated using a MinElute Kit (QIAGEN, Germany). ATAC-seq libraries were first subjected to 5 cycles of preamplification. To determine the suitable number of cycles required for the second round of PCR, the library was assessed by quantitative PCR as described, and the library was then PCR amplified for the appropriate number of cycles. Libraries were purified with a QIAquick PCR (QIAGEN, Germany) column. The library concentration was measured using the KAPA Library Quantification Kit (KK4824) according to the manufacturer's instructions. The library's integrity was checked by gel electrophoresis. Finally, the ATAC library was sequenced on a NextSeq 500 using the NextSeq 500 High Output Kit v2 (150 cycles) (FC-404-2002, Illumina) according to the manufacturer's instructions.

## CUT&Tag sequencing

CUT&Tag experiments were performed using Hyperactive *In-Situ* ChIP LibraryPrep kit for Illumina (TD901-02, Vazyme, China) as

**Table 1. Antibodies and sgRNAs used in this study.**

Targets	Clone	Tag	Vendor	Catalog number	Application
CD3	OKT3	PE-Cy7	Biologend	317334	FACS
CD4	OKT4	APC-Cy7	Biologend	317428	FACS
CD8	RPA-T8	FITC	Biologend	301006	FACS
CD56	5.1H11	PE	Biologend	306722	FACS
NKp30	P30-15	PE	Biologend	325208	FACS
NKp30	P30-15	APC	Biologend	325210	FACS
NKp46	9E2	PE	Biologend	331908	FACS
NKp46	9E2	APC	Biologend	331918	FACS
mIgG1	MOPC-21		Biologend	400101	Control
GAPDH	mAbcam9484		Abcam	ab9484	Western blot
BCL11B	25B6		Abcam	ab18465	Western blot
OPA1	D7C1A		Cell Signaling	67589	Western blot
DRP1	D6C7		Cell Signaling	8570	Western blot
MFN1	D6E2S		Cell Signaling	14739	Western blot
MFN2	D2D10		Cell Signaling	9482	Western blot
Tom20	D8T4N		Cell Signaling	42406	Western blot
MTA2	EPR8537(2)		Abcam	Ab171073	Western blot
MBD2	EPR18361		Abcam	Ab188474	Western blot
CHD4	D4B7		Cell Signaling	12011	Western blot
$\beta$ -actin	8H10D10		Cell Signaling	3700	Western blot
$\beta$ -tubulin	D65A4		Cell Signaling	5666	Western blot
H3K27Ac	D5E4		Cell Signaling	15485	Western blot
H3	D1H2		Cell Signaling	60932SF	Western blot
MBD2	106B691		Abcam	Ab45027	Cut&Tag
CHD4	D4B7		Cell Signaling	12011	Cut&Tag
BCL11B	D6F1		Cell Signaling	12120s	Cut&tag
H3K27Ac	Polyclonal		Activemotif	39133	Cut&tag
sg- <i>BCL11B</i>	GAAGCAGTGTGGCGGCAGCT		GGTCAGACGGAGGCTCCCTT		Function
sg- <i>OPA1</i>	GCTGGCCAAAATTCCTGCG				Function
sg- <i>MTA2</i>	AGGAGCATAAGGCCGTCGGG		GCAAAGGAACGGCTACGACC		Function
sg- <i>MTA1</i>	AAGTGGTGTGCTTCTACCGG		TGACGTTGTTGACGCTGATT		Function
sg- <i>MBD2</i>	AGCCGGTCCCTTCCCGTCG		AGGGCAAGTCTCCGCTGCTG		Function
sg- <i>CHD4</i>	TGTGGAGGTGCCTATCCGCA		ATGGCTCTGTCCCGTTGTA		Function
sg-Ctrl	CCGGTCTTCGAGAAGACCT				Function

described previously with modifications (Dan *et al.*, 2020). Briefly, 100,000 cells were incubated with activated concanavalin A-coated magnetic beads. The bead-bound cells were permeabilized and incubated first with primary antibody, followed by secondary antibody. Diluted pG-Tn5 adaptor complex was then added followed by the tagmentation reaction. Extracted DNA fragments were used for library preparation. Finally, the CUT&Tag library was sequenced on the Illumina NovaSeq platform at Novogene Co., LTD.

#### Acetyl-CoA and $\alpha$ -KG measurement

Acetyl-CoA levels were measured using PicoProbe™ Acetyl CoA Fluorometric Assay Kit (#K317-100, BioVision, Milpitas, CA, USA).

Briefly, 1,000,000 cells were washed with PBS and lysed with acetyl-CoA assay buffer on ice. Then the supernatant was collected by centrifugation (10,000  $g \times 10$  min, 4°C). Ten microliters of CoA Quencher were added to each sample to correct for background followed by 2  $\mu$ l of quencher remover. Fifty microliters of acetyl-CoA reaction mixture containing the Substrate Mix, Conversion Enzyme, Enzyme mix, and PicoProbe were subsequently added and incubated at 37°C for 30 min. Fluorescence of Excitation/Emission = 535/587 nm was measured. After correction for the matched background well (acetyl-CoA reaction mixture added without conversion enzyme) of all readings, the values for each sample were normalized to the protein concentration in each sample determined using BCA protein assay kit (# E-BC-K318-M, Elabscience).

$\alpha$ -KG levels were measured using  $\alpha$ -KG Colorimetric/Fluorometric Assay Kit (#K677-100, BioVision, Milpitas, CA, USA). Briefly,  $2 \times 10^6$  cells are rapidly homogenized with 100  $\mu$ l of ice cold  $\alpha$ -KG assay buffer. Add 1–50  $\mu$ l samples of a 96-well plate and bring volume to 50  $\mu$ l with Assay buffer. Then 50  $\mu$ l the Reaction Mix to each well containing samples and background control. Incubate for 30 min at 37°C and Fluorescence of Excitation/Emission = 535/587 nm was measured.

### In vitro killing assays

The K562-GL and HepG2-GL target cells were incubated with the indicated killing cells at the indicated ratio in triplicate wells of U-bottomed 96-well plates. Target cell viability was monitored 24 h later by adding 100  $\mu$ l of the substrate D-luciferin (potassium salt) (Cayman Chemical, Michigan, USA) at 150  $\mu$ g/ml to each well. Background luminescence was negligible (< 1% of the signal from wells containing only target cells). The percent cytotoxicity (killing %) values were calculated as (blank signal – experimental signal)/blank signal  $\times$  100%.

### Cytokine release assays

Cytokine secretion profiles of indicated killing cells were incubated with cancer cells at an E:T ratio of 1:1 for 24 h. Hundred microliters of supernatants were then collected and stored at –20°C for further measurement. The concentration of cytokines was quantified by enzyme-linked immunosorbent assay (ELISA) according to manufacturers' protocols. ELISA kits for human IFN- $\gamma$ , Granzyme B, and GM-CSF were purchased from Thermo Fisher Scientific Inc, USA.

### Extracellular metabolic flux analysis

For the mitochondria stress test, OCR was measured using a 24-well XFe Analyzer system (Seahorse Bioscience). Indicated cells ( $2 \times 10^5$  cells/well) were plated on pretreated Seahorse plates (BD Biosciences) in XF media (10 mM glucose, 2 mM glutamine and 1 mM pyruvate). Basal OCR was measured for 30 min. Cells were cocultured with 2  $\mu$ M oligomycin, 1  $\mu$ M FCCP, and 1  $\mu$ M each of rotenone and antimycin A (all drugs were from Agilent Technologies), to measure maximal respiration and spare respiratory capacity (SRC = maximal respiration-basal respiration).

### Metabolic assays

For analysis of mitochondrial mass, fresh cells were stained with 200 nM MitoTracker Green in culture medium for 30 min at 37°C. For measurement of the mitochondrial membrane potential, fresh cells were stained with 100 nM TMRM in culture medium for 10 min at 37°C. For measurement of mitochondrial superoxide production, fresh cells were incubated with 10  $\mu$ M MitoSOX in culture medium for 20 min at 37°C. After washing twice with preheated PBS, cells were surface-stained and measured by flow cytometry.

### Real-time PCR

Total RNA was prepared with FastPure Cell/Tissue Total RNA Isolation Kit V2 (RC112-01, Vazyme, China) according to the

manufacturer's instructions. cDNA was reverse transcribed from mRNA with TransScript Uni All-in One First-Strand Cdna Synthesis SuperMix for qPCR kit (AU341, TransGene, China). qPCR was performed with TransStart Tip Green qPCR SuperMix (AQ141, TransGene, China) on a Bio-Rad CFX96 real-time PCR machine (Bio-Rad, Hercules, CA). The primers are listed in Table 2.

### ChIP-qPCR

Cell lysis, sonication, and immunoprecipitation were performed using the SimpleChIP Enzymatic Chromatin IP Kit (Magnetic Beads) (Cell Signaling Technology, 9003S) according to the manufacturer's instructions. The antibodies for immunoprecipitation were acetyl-histone H3 (Lys27) (Cell Signaling Technology, no. 8173, 1:100) and IgG (Cell Signaling Technology, no. 2729, 1:100). All reactions were performed with TransStart Tip Green qPCR SuperMix (AQ141, TransGene, China) on a Bio-Rad CFX96 real-time PCR machine (Bio-Rad, Hercules, CA). The ChIP-qPCR primers are listed in Table 2.

### CUT&Tag qPCR

CUT&Tag experiments were performed using Hyperactive *In-Situ* ChIP LibraryPrep kit for Illumina (TD901-02, Vazyme, China) as described above. The extracted DNA fragments were performed by PCR amplification. The PCR products were purified and then performed with TransStart Tip Green qPCR SuperMix (AQ141, TransGene, China) on a Bio-Rad CFX96 real-time PCR machine (Bio-Rad, Hercules, CA). Twenty nanograms of DNA library were used for each PCR reaction. The CUT&Tag-qPCR primers are listed in Table 3.

**Table 2. Primers for ChIP-qPCR and RT-qPCR.**

Genes	Forward primer 5' → 3'	Reverse primer 5' → 3'
OPA1	ATGTGGCGACTACGTCGGG	TTTCTCCTGATGAAGAGCTT
ID2	GCTATACAACATGAACGACTGCT	AATAGTGGGATGCGAGTCCAG
ZBTB16	GAGATCCTCTCCACCGCAAT	CCGCATACAGCAGGTCATC
NCR1	CTAGGCCGGCAGAATCTGAG	TTTGGGAGAGTCTGCTGCTG
NCR2	TTCCCTGTGCCACAGAATC	CCTGGAGAAGACTGGGAGA
NCR3	TACAGTCTCCTCCTTCGGG	TTCCAGGTGAGACATTTGCC
GZMB	ACCAATCCTGCTTCTGCTGG	GTGGAGAAAGGGCAGGAGAC
IFN $\gamma$	AGAAACCTGTACCATTGGGGG	AGCTCAACAAGCTGATACTCCA
CSF2	GACACTGCTGCTGAGATGGT	TATCAAGCTGACAGGCGTGG
EEF2	TGAACAAGATGGACCGCG	GGATCGATCATGATGTTGCC
B2M	GATGAGTATGCCTGCCGTGT	TGGCGCATCTTCAAACCTCC
MYH9	AAGAACAAGCTCAGGCGC	GCTGTGGTGTCTGTCTGTCC
TUBB	CCACCGGCACCTACCAC	CTGCCCAGACTGACCAAAT
TCF7	TTGATGCTAGGTTCTGGTGATACC	CCTTGGACTCTGCTGTGTGC
LEF1	TTCTTGGCAGAAGGTGGCAT	AGGCAGCTGCTATTCTTGGA
CCR7	ACAGCCTTCTGTGTGGTTT	CTTGACACAGGCATACCTGGAA
BCL11B	TCCAGTACATTTGCACAACA	GCTCCAGGTAGATGCGGAAG

The sequences of primers used in this study.



**Table 3. Primers for CUT&Tag-qPCR.**

Genes	Forward primer 5' → 3'	Reverse primer 5' → 3'
OPA1 Primer 1	GGCTCTTGCGGAAGTCCAT	GGAATGACCCAGGAAGTGGC
OPA1 Primer 2	GCCACTTCTGGGTCATTCC	GACGTAGTCGCCACATCCC
OPA1 Primer 3	GCTCTGTCCATGAGTCACCT	GGTAGGGAAAGAGACGGAC
OPA1 Primer 4	GCTCATTGTTGCAGGCATTTGA	ATGCATTCCATTCTTATAACACG
OPA1 Primer 5	AGCATTCTCTGTTGGAGCAAT	TGCCATCACCAGGAGACATTT
OPA1 Primer 6	CCTCCCACTCCCTTTGGATAC	AGGAAATTCGCCAGGACATAAAAT
ID2	GCTATACAACATGAACGACTGCT	AATAGTGGGATCGGAGTCCAG
ZBTB16	GAGATCTCTTCCACCGCAAT	CCGCATACAGCAGGTCATC
ZNF683	CACCCACCTGTTACCTATG	CCCCAGCTCATTGACCATCA

The sequences of primers used in this study.

### Bulk RNA sequencing

mRNA extracted from purified T cells (purity > 90%) transduced with sgCtrl, *sgBCL11B*, *sgMTA2*, *sgMBD2*, or *sgCHD4* from CD4 and CD8 T cell populations was performed on a BGISEQ-500 (Mak et al, 2017) (BGI, Wuhan, China). Sequenced reads were trimmed for adaptor sequences and masked for low-complexity or low-quality sequences. The number of raw reads mapped to genes was calculated by RSEM (rsem-1.2.4), and the sample results were combined and normalized by EDASEQ (1.99.1). Gene expression fold changes were calculated using normalized raw reads. The downstream analysis used glbase scripts. Gene differential expression analysis was performed by R package DESeq2 (version 1.38.1). The number of differentially expressed genes was counted as visualized by customized R scripts using ggplot2 (version 3.4.0). Gene Ontology (G.O.) enrichment analysis was performed by R package clusterprofile (version 4.6.2). The was visualized as heatmaps generated by customized R scripts using ggplot2 (version 3.4.0).

### CUT&Tag-seq and ATAC-seq data analysis

The sequencing Raw reads were processed by fastp (version 0.20.1) to filter out bad reads and cut adapters. Clean reads were aligned to the human genome defined by NCBI (GCF\_000001405.40) with bowtie2 (version 2.2.5). Aligned reads were indexed and sorted with samtools (version 1.3.1). PCR duplicates were removed using the “markdup” function of sambamba (version 4.2.0.0). MACS2 (version 2.2.7.1) was used for peakcalling, blacklist region of the human genome was excluded from peakcalling results. Homer (version 4.11.1) was used to annotate peaks to genomic regions. DeepTools (version 3.5.1) was used to calculate scores per genome regions of interesting and create heatmaps for scores associated with genomic regions. The bedGraphToBigWig (version 2.9) was used to convert bedGraph file to bigwig format. BigWig tracks were visualized in the Integrative Genomic Viewer genome (IGV) browser (version 2.8.12).

### Statistics

Statistical significance was determined using Student's *t*-test (two groups) or ANOVA with Tukey, Sidak, and Dunnett's multiple

comparison test (three or more groups). All statistical analyses were performed using Prism version 7.0 (GraphPad, Inc., San Diego, CA, USA). \**P* ≤ 0.05, \*\**P* ≤ 0.01, \*\*\**P* ≤ 0.001, and \*\*\*\**P* ≤ 0.0001 were considered statistically significant.

### Data availability

The raw sequence data reported in this paper have been deposited in the Genome Sequence Archive (Chen et al, 2021) in National Genomics Data Center (CNGB-NGDC Members and Partners, 2022), China National Center for Bioinformatics/Beijing Institute of Genomics, Chinese Academy of Sciences (GSA-Human: HRA004801) that are publicly accessible at <https://ngdc.cnbc.ac.cn/gsa-human>.

**Expanded View** for this article is available [online](#).

### Acknowledgements

We thank Diwei Zheng, Yuanbin Cui, Qiting Wu, Youguo Long, Suna Wang, Shouheng Lin, and Duo Hu for their help and contributions to this study. We also thank the teams at the Analysis and Test Center of GIBH for their invaluable support in providing core facilities for our research. This study was supported by the National Key Research and Development Plan, No. 2021YFE0202800 (PL), 2017YFE0131600 (YL); National Natural Science Foundation of China, No. 81972672 (PL), 32170946 (ZJ), 82003054 (SL), 82273377 (SL), 82202031 (LQ); The Youth Innovation Promotion Association of the Chinese Academy of Sciences (2020351, ZJ); 2021355, YW); Guangdong Natural Science Foundation, No. 2022A1515012569 (ZJ), 2022A1515012484 (SL), 2021A1515220077 (SL), 2021A1515110005 (LQ), 2022A1515012360 (LQ), 2022A1515010604 (YY), 2022A1515110349 (DZ); 2020B1212060052; Science and Technology Program of Guangzhou, No. 202102080470 (YY), 2023A04J0103 (RL). Partially supported by a grant from the University Grants Committee/Research Grants Council of the Hong Kong Special Administrative Region, China (Project No. AoE/M-401/20), Innovation and Technology Fund (ITF).

### Author contributions

**Peng Li:** Conceptualization; resources; data curation; supervision; funding acquisition; investigation; writing – original draft; project administration; writing – review and editing. **Rui Liao:** Conceptualization; data curation; formal analysis; validation; investigation; visualization; methodology; writing – original draft; writing – review and editing. **Yi Wu:** Data curation; formal

analysis; funding acquisition; validation; investigation; visualization; methodology; writing – review and editing. **Le Qin:** Funding acquisition; methodology. **Zhiwu Jiang:** Funding acquisition; investigation; methodology. **Shixue Gou:** Formal analysis; validation; methodology. **Linfu Zhou:** Formal analysis; validation; methodology. **Qilan Hong:** Formal analysis. **Yao Li:** Validation; methodology. **Jingxuan Shi:** Formal analysis; validation. **Yao Yao:** Funding acquisition. **Liangxue Lai:** Resources. **Yangqiu Li:** Resources; funding acquisition. **Pentao Liu:** Resources. **Jean Paul Thiery:** Resources; writing – review and editing. **Dajiang Qin:** Resources. **Thomas Graf:** Resources; writing – review and editing. **Xingguo Liu:** Conceptualization; resources; data curation; supervision; project administration; writing – review and editing.

## Disclosure and competing interests statement

The authors declare that they have no conflict of interest.

## References

- Anand R, Wai T, Baker MJ, Kladt N, Schauss AC, Rugarli E, Langer T (2014) The i-AAA protease YME1L and OMA1 cleave OPA1 to balance mitochondrial fusion and fission. *J Cell Biol* 204: 919–929
- Baixauli F, Piletic K, Puleston DJ, Villa M, Field CS, Flachsmann LJ, Quintana A, Rana N, Edwards-Hicks J, Matsushita M *et al* (2022) An LKB1-mitochondria axis controls T<sub>H</sub>17 effector function. *Nature* 610: 555–561
- Baker MJ, Lampe PA, Stojanovski D, Korwitz A, Anand R, Tatsuta T, Langer T (2014) Stress-induced OMA1 activation and autocatalytic turnover regulate OPA1-dependent mitochondrial dynamics. *EMBO J* 33: 578–593
- Buck MD, O'Sullivan D, Klein Geltink RI, Curtis JD, Chang CH, Sanin DE, Qiu J, Kretz O, Braas D, van der Windt GJ *et al* (2016) Mitochondrial dynamics controls T cell fate through metabolic programming. *Cell* 166: 63–76
- Califano D, Sweeney KJ, Le H, VanValkenburgh J, Yager E, O'Connor W Jr, Kennedy JS, Jones DM, Avram D (2014) Diverting T helper cell trafficking through increased plasticity attenuates autoimmune encephalomyelitis. *J Clin Invest* 124: 174–187
- Chang CH, Curtis JD, Maggi LB Jr, Faubert B, Villarino AV, O'Sullivan D, Huang SC, van der Windt GJ, Blagih J, Qiu J *et al* (2013) Posttranscriptional control of T cell effector function by aerobic glycolysis. *Cell* 153: 1239–1251
- Chen H, Detmer SA, Ewald AJ, Griffin EE, Fraser SE, Chan DC (2003) Mitofusins Mfn1 and Mfn2 coordinately regulate mitochondrial fusion and are essential for embryonic development. *J Cell Biol* 160: 189–200
- Chen T, Chen X, Zhang S, Zhu J, Tang B, Wang A, Dong L, Zhang Z, Yu C, Sun Y *et al* (2021) The genome sequence archive family: toward explosive data growth and diverse data types. *Genomics Proteomics Bioinformatics* 19: 578–583
- Cismasiu VB, Adamo K, Gecewicz J, Duque J, Lin Q, Avram D (2005) BCL11B functionally associates with the NuRD complex in T lymphocytes to repress targeted promoter. *Oncogene* 24: 6753–6764
- Cismasiu VB, Paskaleva E, Suman Daya S, Canki M, Duus K, Avram D (2008) BCL11B is a general transcriptional repressor of the HIV-1 long terminal repeat in T lymphocytes through recruitment of the NuRD complex. *Virology* 380: 173–181
- CNCB-NGDC Members and Partners (2022) Database resources of the national genomics data center, China National Center for bioinformatics in 2022. *Nucleic Acids Res* 50: D27–D38
- Constantinides MG, McDonald BD, Verhoef PA, Bendelac A (2014) A committed precursor to innate lymphoid cells. *Nature* 508: 397–401
- Dan L, Liu L, Sun Y, Song J, Yin Q, Zhang G, Qi F, Hu Z, Yang Z, Zhou Z *et al* (2020) The phosphatase PAC1 acts as a T cell suppressor and attenuates host antitumor immunity. *Nat Immunol* 21: 287–297
- Dege C, Hagman J (2014) Mi-2/NuRD chromatin remodeling complexes regulate B and T-lymphocyte development and function. *Immunol Rev* 261: 126–140
- Del Dotto V, Mishra P, Vidoni S, Fogazza M, Maresca A, Caporali L, McCaffery JM, Cappelletti M, Baruffini E, Lenaers G *et al* (2017) OPA1 isoforms in the hierarchical organization of mitochondrial functions. *Cell Rep* 19: 2557–2571
- Del Dotto V, Fogazza M, Carelli V, Rugolo M, Zanna C (2018) Eight human OPA1 isoforms, long and short: what are they for? *Biochim Biophys Acta Bioenerg* 1859: 263–269
- Delconte RB, Shi W, Sathe P, Ushiki T, Seillet C, Minnich M, Kolesnik TB, Rankin LC, Mielke LA, Zhang JG *et al* (2016) The helix-loop-helix protein ID2 governs NK cell fate by tuning their sensitivity to interleukin-15. *Immunity* 44: 103–115
- Dimeloe S, Burgener AV, Grahlert J, Hess C (2017) T-cell metabolism governing activation, proliferation and differentiation; a modular view. *Immunology* 150: 35–44
- Ding M, Liu C, Shi R, Yu M, Zeng K, Kang J, Fu F, Mi M (2020) Mitochondrial fusion promoter restores mitochondrial dynamics balance and ameliorates diabetic cardiomyopathy in an optic atrophy 1-dependent way. *Acta Physiol* 229: e13428
- Dubuissez M, Loison I, Paget S, Vorng H, Ait-Yahia S, Rohr O, Tscoupoulos A, Leprince D (2016) Protein kinase C-mediated phosphorylation of BCL11B at serine 2 negatively regulates its interaction with NuRD complexes during CD4<sup>+</sup> T-cell activation. *Mol Cell Biol* 36: 1881–1898
- Durbin AD, Wang T, Wimalasena VK, Zimmerman MW, Li D, Dharia NV, Mariani L, Shendy NAM, Nance S, Patel AG *et al* (2022) EP300 selectively controls the enhancer landscape of MYCN-amplified neuroblastoma. *Cancer Discov* 12: 730–751
- Ehse S, Raschke I, Mancuso G, Bernacchia A, Geimer S, Tondera D, Martinou JC, Westermann B, Rugarli EI, Langer T (2009) Regulation of OPA1 processing and mitochondrial fusion by m-AAA protease isoenzymes and OMA1. *J Cell Biol* 187: 1023–1036
- Fanucchi S, Domínguez-Andrés J, Joosten LAB, Netea MG, Mhlanga MM (2021) The intersection of epigenetics and metabolism in trained immunity. *Immunity* 54: 32–43
- Gao Q, Tian R, Han H, Slone J, Wang C, Ke X, Zhang T, Li X, He Y, Liao P *et al* (2022a) PINK1-mediated Drp1<sup>S616</sup> phosphorylation modulates synaptic development and plasticity via promoting mitochondrial fission. *Signal Transduct Target Ther* 7: 103
- Gao Y, Zamisch M, Vacchio M, Chopp L, Ciucci T, Paine EL, Lyons GC, Nie J, Xiao Q, Zvezdova E *et al* (2022b) NuRD complex recruitment to Thpok mediates CD4<sup>+</sup> T cell lineage differentiation. *Sci Immunol* 7: eabn5917
- Ge Y, Shi X, Boopathy S, McDonald J, Smith AW, Chao LH (2020) Two forms of Opa1 cooperate to complete fusion of the mitochondrial inner-membrane. *Elife* 9: e50973
- Ghesquière B, Wong BW, Kuchnio A, Carmeliet P (2014) Metabolism of stromal and immune cells in health and disease. *Nature* 511: 167–176
- Gripic L, Kanazawa T, van der Bliek AM (2007) Regulation of the mitochondrial dynamin-like protein Opa1 by proteolytic cleavage. *J Cell Biol* 178: 757–764
- Hosokawa H, Romero-Wolf M, Yui MA, Ungerback J, Quilooan MLG, Matsumoto M, Nakayama KI, Tanaka T, Rothenberg EV (2018) Bcl11b sets pro-T cell fate by site-specific cofactor recruitment and by repressing Id2 and Zbtb16. *Nat Immunol* 19: 1427–1440

- Hosokawa H, Romero-Wolf M, Yang Q, Motomura Y, Levanon D, Groner Y, Moro K, Tanaka T, Rothenberg EV (2020) Cell type-specific actions of Bcl11b in early T-lineage and group 2 innate lymphoid cells. *J Exp Med* 217: e20190972
- Hu G, Cui K, Fang D, Hirose S, Wang X, Wangsa D, Jin W, Ried T, Liu P, Zhu J et al (2018) Transformation of accessible chromatin and 3D nucleome underlies lineage commitment of early T cells. *Immunity* 48: 227–242
- Ikawa T, Hirose S, Masuda K, Kakugawa K, Satoh R, Shibano-Satoh A, Kominami R, Katsura Y, Kawamoto H (2010) An essential developmental checkpoint for production of the T cell lineage. *Science* 329: 93–96
- Ishihara N, Fujita Y, Oka T, Mihara K (2006) Regulation of mitochondrial morphology through proteolytic cleavage of OPA1. *EMBO J* 25: 2966–2977
- Isoda T, Moore AJ, He Z, Chandra V, Aida M, Denholtz M, Piet van Hamburg J, Fisch KM, Chang AN, Fahl SP et al (2017) Non-coding transcription instructs chromatin folding and compartmentalization to dictate enhancer-promoter communication and T cell fate. *Cell* 171: 103–119
- Jiang Z, Qin L, Tang Y, Liao R, Shi J, He B, Li S, Zheng D, Cui Y, Wu Q et al (2022) Human induced-T-to-natural killer cells have potent anti-tumour activities. *Biomark Res* 10: 13
- Juno JA, van Bockel D, Kent SJ, Kelleher AD, Zaunders JJ, Munier CM (2017) Cytotoxic CD4 T cells—friend or foe during viral infection? *Front Immunol* 8: 19
- Kishton RJ, Sukumar M, Restifo NP (2017) Metabolic regulation of T cell longevity and function in tumor immunotherapy. *Cell Metab* 26: 94–109
- Li L, Leid M, Rothenberg EV (2010a) An early T cell lineage commitment checkpoint dependent on the transcription factor Bcl11b. *Science* 329: 89–93
- Li P, Burke S, Wang J, Chen X, Ortiz M, Lee SC, Lu D, Campos L, Goulding D, Ng BL et al (2010b) Reprogramming of T cells to natural killer-like cells upon Bcl11b deletion. *Science* 329: 85–89
- Li D, Liu J, Yang X, Zhou C, Guo J, Wu C, Qin Y, Guo L, He J, Yu S et al (2017) Chromatin accessibility dynamics during iPSC reprogramming. *Cell Stem Cell* 21: 819–833
- Liu PS, Wang H, Li X, Chao T, Teav T, Christen S, Di Conza G, Cheng WC, Chou CH, Vavakova M et al (2017)  $\alpha$ -ketoglutarate orchestrates macrophage activation through metabolic and epigenetic reprogramming. *Nat Immunol* 18: 985–994
- Lorentsen KJ, Cho JJ, Luo X, Zuniga AN, Urban JF Jr, Zhou L, Gharaibeh R, Jobin C, Kladde MP, Avram D (2018) Bcl11b is essential for licensing Th2 differentiation during helminth infection and allergic asthma. *Nat Commun* 9: 1679
- Losón OC, Song Z, Chen H, Chan DC (2013) Fis1, Mff, MiD49, and MiD51 mediate Drp1 recruitment in mitochondrial fission. *Mol Biol Cell* 24: 659–667
- Loughran SJ, Comoglio F, Hamey FK, Giustacchini A, Errami Y, Earp E, Göttgens B, Jacobsen SEW, Mead AJ, Hendrich B et al (2017) Mbd3/NuRD controls lymphoid cell fate and inhibits tumorigenesis by repressing a B cell transcriptional program. *J Exp Med* 214: 3085–3104
- Louis C, Souza-Fonseca-Guimaraes F, Yang Y, D'Silva D, Kratina T, Dagley L, Hediye-Zadeh S, Rautela J, Masters SL, Davis MJ et al (2020) NK cell-derived GM-CSF potentiates inflammatory arthritis and is negatively regulated by CIS. *J Exp Med* 217: e20191421
- Lu X, Kovalev GI, Chang H, Kallin E, Knudsen G, Xia L, Mishra N, Ruiz P, Li E, Su L et al (2008) Inactivation of NuRD component Mta2 causes abnormal T cell activation and lupus-like autoimmune disease in mice. *J Biol Chem* 283: 13825–13833
- MacIver NJ, Michalek RD, Rathmell JC (2013) Metabolic regulation of T lymphocytes. *Annu Rev Immunol* 31: 259–283
- Mak SST, Gopalakrishnan S, Caroe C, Geng C, Liu S, Sinding MS, Kuderna LFK, Zhang W, Fu S, Vieira FG et al (2017) Comparative performance of the BGISEQ-500 vs Illumina HiSeq2500 sequencing platforms for palaeogenomic sequencing. *Gigascience* 6: 1–13
- Maluski M, Ghosh A, Herbst J, Scholl V, Baumann R, Huehn J, Geffers R, Meyer J, Maul H, Eiz-Vesper B et al (2019) Chimeric antigen receptor-induced BCL11B suppression propagates NK-like cell development. *J Clin Invest* 129: 5108–5122
- Matilainen O, Quirós PM, Auwerx J (2017) Mitochondria and epigenetics - crosstalk in homeostasis and stress. *Trends Cell Biol* 27: 453–463
- Morris JP 4th, Yashinski JJ, Koche R, Chandwani R, Tian S, Chen CC, Baslan T, Marinkovic ZS, Sánchez-Rivera FJ, Leach SD et al (2019)  $\alpha$ -Ketoglutarate links p53 to cell fate during tumour suppression. *Nature* 573: 595–599
- O'Sullivan D, van der Windt GJ, Huang SC, Curtis JD, Chang CH, Buck MD, Qiu J, Smith AM, Lam WY, DiPlato LM et al (2014) Memory CD8<sup>+</sup> T cells use cell-intrinsic lipolysis to support the metabolic programming necessary for development. *Immunity* 41: 75–88
- Patil VS, Madrigal A, Schmiedel BJ, Clarke J, O'Rourke P, de Silva AD, Harris E, Peters B, Seumois G, Weiskopf D et al (2018) Precursors of human CD4<sup>+</sup> cytotoxic T lymphocytes identified by single-cell transcriptome analysis. *Sci Immunol* 3: ean8664
- Pietrocola F, Galluzzi L, Bravo-San Pedro JM, Madeo F, Kroemer G (2015) Acetyl coenzyme A: a central metabolite and second messenger. *Cell Metab* 21: 805–821
- Ron-Harel N, Santos D, Ghergurovich JM, Sage PT, Reddy A, Lovitch SB, Dephore N, Satterstrom FK, Sheffer M, Spinelli JB et al (2016) Mitochondrial biogenesis and proteome remodeling promote one-carbon metabolism for T cell activation. *Cell Metab* 24: 104–117
- Rothenberg EV (2012) Transcriptional drivers of the T-cell lineage program. *Curr Opin Immunol* 24: 132–138
- Sen P, Lan Y, Li CY, Sidoli S, Donahue G, Dou Z, Frederick B, Chen Q, Luense LJ, Garcia BA et al (2019) Histone acetyltransferase p300 induces *de novo* super-enhancers to drive cellular senescence. *Mol Cell* 73: 684–698
- Shen Y, Wei W, Zhou DX (2015) Histone acetylation enzymes coordinate metabolism and gene expression. *Trends Plant Sci* 20: 614–621
- Shen E, Wang Q, Rabe H, Liu W, Cantor H, Leavenworth JW (2018) Chromatin remodeling by the NuRD complex regulates development of follicular helper and regulatory T cells. *Proc Natl Acad Sci USA* 115: 6780–6785
- Sidwell T, Rothenberg EV (2021) Epigenetic dynamics in the function of T-lineage regulatory factor Bcl11b. *Front Immunol* 12: 669498
- Song Z, Chen H, Fiket M, Alexander C, Chan DC (2007) OPA1 processing controls mitochondrial fusion and is regulated by mRNA splicing, membrane potential, and Yme1L. *J Cell Biol* 178: 749–755
- Song Z, Ghochani M, McCaffery JM, Frey TG, Chan DC (2009) Mitofusins and OPA1 mediate sequential steps in mitochondrial membrane fusion. *Mol Biol Cell* 20: 3525–3532
- Sottile R, Panjwani MK, Lau CM, Daniyan AF, Tanaka K, Barker JN, Brentjens RJ, Sun JC, Le Luque JB, Hsu KC (2021) Human cytomegalovirus expands a CD8<sup>+</sup> T cell population with loss of BCL11B expression and gain of NK cell identity. *Sci Immunol* 6: eabe6968
- Stadtmauer EA, Fraietta JA, Davis MM, Cohen AD, Weber KL, Lancaster E, Mangan PA, Kulikovskaya I, Gupta M, Chen F et al (2020) CRISPR-engineered T cells in patients with refractory cancer. *Science* 367: eaba7365
- Sukumar M, Liu J, Ji Y, Subramanian M, Crompton JG, Yu Z, Roychowdhuri R, Palmer DC, Muranski P, Karoly ED et al (2013) Inhibiting glycolytic metabolism enhances CD8<sup>+</sup> T cell memory and antitumor function. *J Clin Invest* 123: 4479–4488

- Sutendra G, Kinnaird A, Dromparis P, Paulin R, Stenson TH, Haromy A, Hashimoto K, Zhang N, Flaim E, Michelakis ED (2014) A nuclear pyruvate dehydrogenase complex is important for the generation of acetyl-CoA and histone acetylation. *Cell* 158: 84–97
- Takeuchi A, Saito T (2017) CD4 CTL, a cytotoxic subset of CD4<sup>+</sup> T Cells, their differentiation and function. *Front Immunol* 8: 194
- Topark-Ngarm A, Golonzhka O, Peterson VJ, Barrett B Jr, Martinez B, Crofoot K, Filtz TM, Leid M (2006) CTIP2 associates with the NuRD complex on the promoter of p57KIP2, a newly identified CTIP2 target gene. *J Biol Chem* 281: 32272–32283
- van der Windt GJ, Everts B, Chang CH, Curtis JD, Freitas TC, Amiel E, Pearce EJ, Pearce EL (2012) Mitochondrial respiratory capacity is a critical regulator of CD8<sup>+</sup> T cell memory development. *Immunity* 36: 68–78
- Wang D, Wang J, Bonamy GM, Meeusen S, Bruschi RG, Turk C, Yang P, Schultz PG (2012) A small molecule promotes mitochondrial fusion in mammalian cells. *Angew Chem Int Ed Engl* 51: 9302–9305
- Wang Y, Huang Y, Liu J, Zhang J, Xu M, You Z, Peng C, Gong Z, Liu W (2020) Acetyltransferase GCN5 regulates autophagy and lysosome biogenesis by targeting TFEB. *EMBO Rep* 21: e48335
- West AP, Shadel GS, Ghosh S (2011) Mitochondria in innate immune responses. *Nat Rev Immunol* 11: 389–402
- Wu Z, Lau CM, Sottile R, Le Luduec JB, Panjwani MK, Conaty PM, Srpan K, Laib Sampaio K, Mertens T, Adler SP et al (2021) Human cytomegalovirus infection promotes expansion of a functionally superior cytoplasmic CD3<sup>+</sup> NK cell subset with a Bcl11b-regulated T cell signature. *J Immunol* 207: 2534–2544
- Wu Y, Chen K, Li L, Hao Z, Wang T, Liu Y, Xing G, Liu Z, Li H, Yuan H et al (2022) Plin2-mediated lipid droplet mobilization accelerates exit from pluripotency by lipidomic remodeling and histone acetylation. *Cell Death Differ* 29: 2316–2331
- Youle RJ, van der Bliek AM (2012) Mitochondrial fission, fusion, and stress. *Science* 337: 1062–1065
- Yu YR, Imrichova H, Wang H, Chao T, Xiao Z, Gao M, Rincon-Restrepo M, Franco F, Genolet R, Cheng WC et al (2020) Disturbed mitochondrial dynamics in CD8<sup>+</sup> TILs reinforce T cell exhaustion. *Nat Immunol* 21: 1540–1551
- Zhang S, Rozell M, Verma RK, Albu DI, Califano D, VanValkenburgh J, Merchant A, Rangel-Moreno J, Randall TD, Jenkins NA et al (2010) Antigen-specific clonal expansion and cytolytic effector function of CD8<sup>+</sup> T lymphocytes depend on the transcription factor Bcl11b. *J Exp Med* 207: 1687–1699
- Zheng X, Qian Y, Fu B, Jiao D, Jiang Y, Chen P, Shen Y, Zhang H, Sun R, Tian Z et al (2019) Mitochondrial fragmentation limits NK cell-based tumor immunosurveillance. *Nat Immunol* 20: 1656–1667
- Zhou W, Zhao T, Du J, Ji G, Li X, Ji S, Tian W, Wang X, Hao A (2019) TIGAR promotes neural stem cell differentiation through acetyl-CoA-mediated histone acetylation. *Cell Death Dis* 10: 198